Study of proton parton distribution functions at high x using ZEUS data

I. Abt,[19] L. Adamczyk,[7] R. Aggarwal,[3,b] V. Aushev,[17] O. Behnke,[9] U. Behrens,[9] A. Bertolin,[21] I. Bloch,[10] I. Brock,[2] N. H. Brook,[28,m] R. Brugnera,[22] A. Bruni,[1] P. J. Bussey,[11] A. Caldwell,[19] M. Capua,[4] C. D. Catterall,[32] J. Chwastowski,[6] J. Ciborowski,[29,n] R. Ciesielski,[9,d] A. M. Cooper-Sarkar,[20] M. Corradi,[1,a] R. K. Dementiev,[18] S. Dusini,[21] J. Ferrando,[9] B. Foster,[20,j] E. Gallo,[13,k] D. Gangadharan,[14] A. Garfagnini,[22] A. Geiser,[9] L. K. Gladilin,[18] Yu. A. Golubkov,[18] G. Grzelak,[29] C. Gwenlan,[20] D. Hochman,[31] N. Z. Jomhari,[9] I. Kadenko,[17] S. Kananov,[23] U. Karshon,[31] P. Kaur,[3,c] R. Klanner,[13] U. Klein,[9,e] I. A. Korzhavina,[18] N. Kovalchuk,[13] H. Kowalski,[9] O. Kuprash,[9,f] M. Kuze,[25] B. B. Levchenko,[18] A. Levy,[23] B. Löhr,[9] A. Longhin,[22] O. Yu. Lukina,[18] I. Makarenko,[9] J. Malka,[9,g] S. Masciocchi,[12,i] K. Nagano,[15] J. D. Nam,[24] J. Onderwaater,[14,l] Yu. Onishchuk,[17] E. Paul,[2] I. Pidhurskyi,[17] A. Polini,[1] M. Przybycień,[7] A. Quintero,[24] M. Ruspa,[27] D. H. Saxon,[11] U. Schneekloth,[9] T. Schörner-Sadenius,[9] I. Selyuzhenkov,[12] M. Shchedrolosiev,[17] L. M. Shcheglova,[18] I. O. Skillicorn,[11] W. Słomiński,[8] A. Solano,[26] L. Stanco,[21] N. Stefaniuk,[9] P. Stopa,[6] B. Surrow,[24] J. Sztuk-Dambietz,[13,g] E. Tassi,[4] K. Tokushuku,[15] M. Turcato,[13,g] O. Turkot,[9] T. Tymieniecka,[30] A. Verbytskyi,[19] W. A. T. Wan Abdullah,[5] K. Wichmann,[9] M. Wing,[28] S. Yamada,[15] Y. Yamazaki,[16] A. F. Żarnecki,[29] L. Zawiejski,[6] and O. Zenaiev[9,h]

(ZEUS Collaboration)

[1]*INFN Bologna, Bologna, Italy*
[2]*Physikalisches Institut der Universität Bonn, Bonn, Germany*
[3]*Panjab University, Department of Physics, Chandigarh, India*
[4]*Calabria University, Physics Department and INFN, Cosenza, Italy*
[5]*National Centre for Particle Physics, Universiti Malaya, Kuala Lumpur, Malaysia*
[6]*The Henryk Niewodniczanski Institute of Nuclear Physics, Polish Academy of Sciences, Krakow, Poland*
[7]*AGH University of Science and Technology, Faculty of Physics and Applied Computer Science, Krakow, Poland*
[8]*Department of Physics, Jagellonian University, Krakow, Poland*
[9]*Deutsches Elektronen-Synchrotron DESY, Hamburg, Germany*
[10]*Deutsches Elektronen-Synchrotron DESY, Zeuthen, Germany*
[11]*School of Physics and Astronomy, University of Glasgow, Glasgow, United Kingdom*
[12]*GSI Helmholtzzentrum für Schwerionenforschung GmbH, Darmstadt, Germany*
[13]*Hamburg University, Institute of Experimental Physics, Hamburg, Germany*
[14]*Physikalisches Institut of the University of Heidelberg, Heidelberg, Germany*
[15]*Institute of Particle and Nuclear Studies, KEK, Tsukuba, Japan*
[16]*Department of Physics, Kobe University, Kobe, Japan*
[17]*Department of Nuclear Physics, National Taras Shevchenko University of Kyiv, Kyiv, Ukraine*
[18]*Lomonosov Moscow State University, Skobeltsyn Institute of Nuclear Physics, Moscow, Russia*
[19]*Max-Planck-Institut für Physik, München, Germany*
[20]*Department of Physics, University of Oxford, Oxford, United Kingdom*
[21]*INFN Padova, Padova, Italy*
[22]*Dipartimento di Fisica e Astronomia dell' Università and INFN, Padova, Italy*
[23]*Raymond and Beverly Sackler Faculty of Exact Sciences, School of Physics, Tel Aviv University, Tel Aviv, Israel*
[24]*Department of Physics, Temple University, Philadelphia, Pennsylvania 19122, USA*
[25]*Department of Physics, Tokyo Institute of Technology, Tokyo, Japan*
[26]*Università di Torino and INFN, Torino, Italy*
[27]*Università del Piemonte Orientale, Novara, and INFN, Torino, Italy*
[28]*Physics and Astronomy Department, University College London, London, United Kingdom*
[29]*Faculty of Physics, University of Warsaw, Warsaw, Poland*
[30]*National Centre for Nuclear Research, Warsaw, Poland*

[31]*Department of Particle Physics and Astrophysics, Weizmann Institute, Rehovot, Israel*
[32]*Department of Physics, York University, Ontario, Canada*

(Received 20 March 2020; accepted 15 May 2020; published 26 June 2020)

At large values of x, the parton distribution functions (PDFs) of the proton are poorly constrained and there are considerable variations between different global fits. Data at such high x have already been published by the ZEUS Collaboration, but not yet used in PDF extractions. A technique for comparing predictions based on different PDF sets to the observed number of events in the ZEUS data is presented. It is applied to compare predictions from the most commonly used PDFs to published ZEUS data at high Bjorken x. A wide variation is found in the ability of the PDFs to predict the observed results. A scheme for including the ZEUS high-x data in future PDF extractions is discussed.

DOI: 10.1103/PhysRevD.101.112009

I. INTRODUCTION

Important questions related to the nature of the strong interaction can be addressed by studying the structure of particles composed of quarks and gluons. The spatial and momentum distributions of these constituents in a hadron are not understood from first principles owing to theoretical and calculational limitations. Thus, our knowledge stems principally from measurements.

Knowledge of the proton structure is also of great importance, as protons are used to reach the high-energy frontier in particle colliders such as the Large Hadron Collider (LHC). Calculated cross sections for processes involving protons are based on sets of parton distribution functions (PDFs), i.e., quark and gluon distribution functions. These PDFs have been extracted by a number of collaborations by selecting data sets from various experiments. The PDF sets used for making predictions for LHC processes, and a prescription for how uncertainties related to the PDFs are to be evaluated, have been published elsewhere [1,2]. Identifying effects due to new physics beyond the Standard Model at high center-of-mass energies requires precise knowledge of the PDFs at high x, where x is the fractional longitudinal momentum of the struck parton inside the proton. This knowledge is essential for the isolation of some types of new physics.

Most of the data available for $x \geq 0.6$ were obtained in fixed-target experiments in a range of Q^2, the negative 4-momentum-transfer squared, where perturbative quantum chromodynamics (pQCD) may not be fully applicable. The HERA (Hadron-Elektron-Ringanlage) storage ring, where 920 GeV protons collided with 27.5 GeV electrons or positrons, offered an opportunity to probe the region of high Bjorken[1] x at high Q^2 where pQCD and the Dokshitzer-Gribov-Lipatov-Altarelli-Parisi evolution dynamics [3–7] are believed to be reliable. The ZEUS Collaboration published high-x data collected in the period 2004–2007, with integrated luminosities of 187 pb^{-1} for $e^- p$ and 142 pb^{-1} for $e^+ p$ scattering [8]. The data cover the Q^2 range of 650–20000 GeV^2 and the x range of 0.03–1.0.

In the following, predictions based on the principal PDF sets used at the LHC are compared to these ZEUS high-x data. While there is some overlap with data used in other ZEUS publications, a substantial fraction of the high-x data from ZEUS has not been previously used in the extraction of PDFs. Most PDF extractions have used the combined HERA data [9] for their extraction procedures. The combined HERA data are reported as cross sections which are extracted from a combination of ZEUS and H1 data. The combination was based on an agreed binning of the kinematically allowed space. The data discussed in this

[a]Present address: INFN Roma, Rome, Italy.
[b]Present address: DST-Inspire Faculty, Department of Technology, SPPU, Pune, India.
[c]Present address: Sant Longowal Institute of Engineering and Technology, Longowal, Punjab, India.
[d]Present address: Rockefeller University, New York, New York 10065, USA.
[e]Present address: University of Liverpool, Liverpool, United Kingdom.
[f]Present address: University of Freiburg, Freiburg, Germany.
[g]Present address: European X-ray Free-Electron Laser facility GmbH, Hamburg, Germany.
[h]Present address: Hamburg University, Hamburg, Germany.
[i]Also at Physikalisches Institut of the University of Heidelberg, Heidelberg, Germany.
[j]Also at DESY and University of Hamburg.
[k]Also at DESY.
[l]Also at GSI Helmholtzzentrum für Schwerionenforschung GmbH, Darmstadt, Germany.
[m]Present address: University of Bath, Bath, United Kingdom.
[n]Also at Lodz University, Lodz, Poland.

[1]From here on, no distinction is made between x and Bjorken x.

paper uses much finer binning than used in the data combination and extends the reported data to $x = 1$. Both these differences lead to bins with small event counts where standard chi-squared fitting is not appropriate and the use of the Poisson distribution to properly account for statistical fluctuations is required. In this paper, the predictions for the expected numbers of events from the different PDF sets are compared to the numbers observed in the ZEUS data and the results are discussed. Section VI of this paper discusses the high-x points published previously [8] that have overlap with HERA-ZEUS legacy data and procedures for taking the data overlap into account in future PDF extractions.

II. METHOD TO TEST HIGH-x PREDICTIONS

In addition to reduced cross sections, the previous ZEUS publication [8] provides the observed numbers of events in $(\Delta x, \Delta Q^2)$ intervals ("bins"). The evaluation of the probability to have observed these numbers of events according to different PDF sets is discussed in the present paper. The probability, $P(D|\mathrm{PDF}_k)$, for a prediction based on a given PDF set k to predict the data set D is

$$P(D|\mathrm{PDF_k}) = \prod_j \frac{e^{-\nu_{j,k}}\nu_{j,k}^{n_j}}{n_j!}, \tag{1}$$

where the index j labels the bins in $(\Delta x, \Delta Q^2)$, $\nu_{j,k}$ is the expected number of events in bin j as predicted from PDF set k, and n_j is the observed number of events. The effect of systematic uncertainties is evaluated by varying the predictions $\nu_{j,k}$ according to the sources of systematic uncertainty as described in Sec. V below.

The probability values in Eq. (1) are very small absolute quantities and only the ratio of probabilities for the different PDF sets are of interest; i.e., the Bayes factors. Using these, an effective $\Delta\chi^2$ between two different PDF sets, here labeled k, l, is defined via

$$\Delta\chi^2_{k,l} = -2\ln\frac{P(D|\mathrm{PDF}_k)}{P(D|\mathrm{PDF}_l)}. \tag{2}$$

These quantities are used to evaluate the relative goodness-of-fit of the different PDF sets. The tail-area probabilities (p-values [10]) for the different PDF sets are also provided, based on the expected probability distribution of the quantities $P(D|\mathrm{PDF}_k)$. These are used to evaluate the overall goodness-of-fit for the prediction based on the PDF set.

To calculate the probabilities as outlined above, the predictions from the PDF sets must be evaluated. The PDFs are used as input to calculate cross sections for the $e^\pm p \to e^\pm X$ neutral current cross sections at the Born level with fixed fine structure constant, $\alpha(Q^2 = 0)$. The predictions for the observed number of events in measured kinematic variables, $(x_{\mathrm{rec}}, Q^2_{\mathrm{rec}})$, are given by integrating over the full kinematic phase space,

$$\nu_{j,k} = \mathcal{L}\int_{(\Delta x,\Delta Q^2)_j}\left[\int A(x_{\mathrm{rec}}, Q^2_{\mathrm{rec}}|x, Q^2) \times \frac{d^2\sigma(x, Q^2|\mathrm{PDF}_k)}{dxdQ^2}dxdQ^2\right]dx_{\mathrm{rec}}dQ^2_{\mathrm{rec}}. \tag{3}$$

Here, $\mathcal{L}$ is the luminosity, $\frac{d^2\sigma(x,Q^2|\mathrm{PDF}_k)}{dxdQ^2}$ is the differential cross section at (x, Q^2) for PDF set k using kinematic quantities defined at the Born level, and $A(x_{\mathrm{rec}}, Q^2_{\mathrm{rec}}|x, Q^2)$ transforms the Born-level cross sections to observed cross sections including all relevant effects (radiative corrections, detector resolution and acceptance, selection criteria, etc.). This integral is approximated as

$$\nu_{j,k} \approx \sum_i A_{ji}\lambda_{i,k}, \tag{4}$$

where $\lambda_{i,k}$ is the expected number of events for the ith $(\Delta x, \Delta Q^2)$ bin at the Born level for PDF set k, and A_{ji} gives the transformation to the expectation in the measured quantities in bin j. In the following, $\boldsymbol{\lambda}_k$ represent the vectors $\{\lambda_{i,k}\}$ and $\boldsymbol{\nu}_k$ the $\{\nu_{j,k}\}$. For the prediction in Eq. (4) to be accurate and sufficiently precise, it is necessary to have sufficiently fine binning and to account for all effects through reliable simulation packages. Thus, the bins defined at the Born level are not identical to those used in the measurements; the index i spans a larger range than the index j.

The matrix $\boldsymbol{A}$ (with components A_{ji}) was decomposed into a matrix representing the QED and QCD radiative effects, $\boldsymbol{R}$, and a matrix, $\boldsymbol{T}$, representing the ZEUS specific detector effects,

$$\boldsymbol{A} = \boldsymbol{TR}. \tag{5}$$

The effects of QED and QCD radiative corrections, including the running of the coupling constants, were determined by running dedicated simulation programs which provide predictions at the "generator level." The matrix $\boldsymbol{R}$ transforms the Born-level quantities, $\lambda_{i,k}$, to the generator-level quantities, $\mu_{l,k}$,

$$\mu_{l,k} = \sum_i R_{li}\lambda_{i,k}, \tag{6}$$

where the same binning was used for $\mu_{l,k}$ and $\lambda_{i,k}$.

The matrix $\boldsymbol{T}$ provides the transformation of the generator-level quantities to the observed quantities. It accounts for all experimental and analysis-related effects, and is, in principle, independent of the PDF set used in the generation of the Monte Carlo simulated events.

Given the notation above, for a given PDF set k, the vector $\boldsymbol{\nu}_k$ is given as

$$\boldsymbol{\nu}_k = \boldsymbol{T\mu}_k, \tag{7}$$

where

$$\boldsymbol{\mu}_k = \boldsymbol{R}\boldsymbol{\lambda}_k. \tag{8}$$

III. EVALUATION OF R AND T

A. Monte Carlo samples

The event simulation was performed using the HERACLES [11] event generator together with the NLO CTEQ5D [12] PDF set, which is extracted using the zero-mass convention for heavy flavors. The HERACLES program applies $O(\alpha)$ QED and $O(\alpha_s)$ QCD corrections, where α_s is the strong coupling constant. The QCD simulation is based on a combination of ARIADNE4.12 [13] and MEPS6.5.1 [14] parton-shower simulations as used in the ZEUS high-x analysis [8]. The detector simulation was carried out using GEANT3.21 [15] tuned to match the ZEUS detector performance. Exactly the same analysis steps that were carried out in the extraction of the observed event numbers [8] were applied in the extraction of the Monte Carlo (MC) event numbers.

The MC events were produced in sets with different minimum Q^2 values in order to have sufficient statistical precision at the highest-x and highest-Q^2 values. The MC event sets were then combined to produce the final sample. This necessitated the introduction of MC event weights, ω^{MC}, to ensure the correct overall cross section, $\frac{d^2\sigma(x,Q^2)}{dxdQ^2}$, as a function of the kinematic variables. Event weights were also introduced in order to improve the MC description of various experimental quantities such as the event-vertex distribution and selection-cut efficiencies [8]. The product of these weights is denoted as ω^{sim}. The total weight for an event m is then $\omega_m = \omega_m^{\mathrm{MC}}\omega_m^{\mathrm{sim}}$.

B. Determination of matrix elements

The ZEUS analysis [8] used 153 $(\Delta x, \Delta Q^2)$ bins, fixing the size of the vector $\boldsymbol{\nu}_k$. The bins for the event-generator quantities were chosen on a finer scale and also extend beyond the kinematic region covered in the measured variables in order to capture all "migrations" from the generated to the measured quantities. Stable results for the predictions were obtained by choosing 429 bins for the $\boldsymbol{\lambda}_k$ and $\boldsymbol{\mu}_k$ vectors, so that the matrix $\boldsymbol{T}$ has 153×429 entries. In particular, it was verified that the predictions for the expected event numbers $\boldsymbol{\nu}_{k=\mathrm{CTEQ5D}}$ as found in the original analysis [8] were reproduced.

The matrix $\boldsymbol{R}$ is a diagonal 429×429 matrix whose elements were evaluated as

$$R_{ii} = \frac{\sum_{m=1}^{M_i} \omega_m^{\mathrm{MC}}}{\mathcal{L}^{\mathrm{MC}}\sigma_{i,\mathrm{CTEQ5D}}}, \tag{9}$$

where M_i is the number of generated events in the ith $(\Delta x, \Delta Q^2)$ bin, with the kinematic quantities calculated using the four-vectors of the exchanged boson and incoming proton, and $\mathcal{L}^{\mathrm{MC}}$ and $\sigma_{i,\mathrm{CTEQ5D}}$ are the MC luminosity and Born-level cross section for bin i. Nondiagonal elements of $\boldsymbol{R}$ were set to zero. It was verified that this simplified treatment of the radiative corrections is adequate for the purposes of this analysis and that $\boldsymbol{R}$ does not depend on the PDF set.

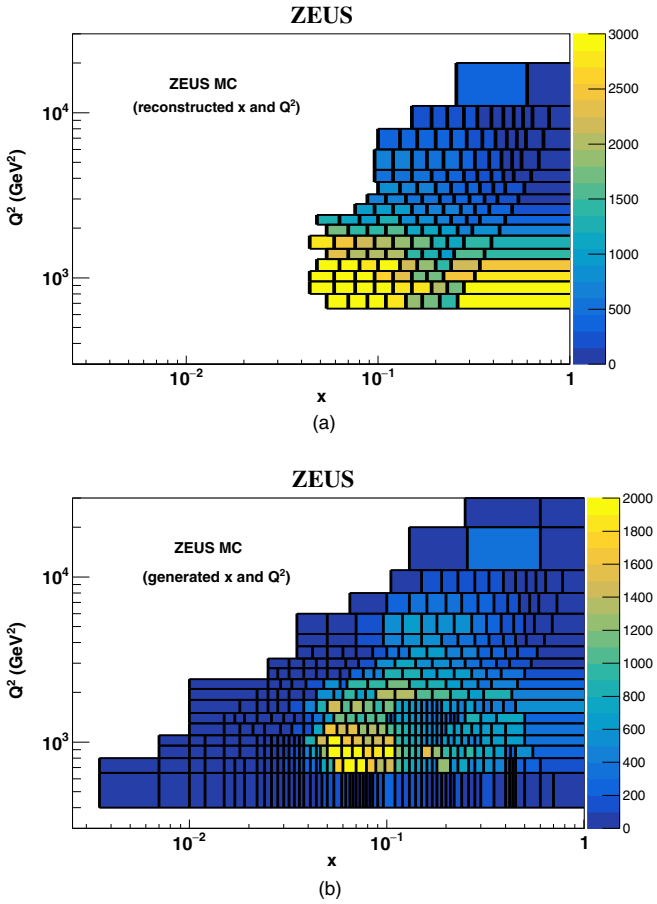

FIG. 1. (a) Distribution of the expected event numbers $\boldsymbol{\nu}_k$ in the Monte Carlo simulation after all analysis selections are applied, shown in bins of the measured quantities. (b) Distribution of the same events, shown in bins of the generated kinematic quantities $\boldsymbol{\mu}_k$.

The elements of $\boldsymbol{T}$ were calculated as

$$T_{ji} = \frac{\sum_{m=1}^{M_i} \omega_m I(m \in j)}{\sum_{m=1}^{M_i} \omega_m^{\mathrm{MC}}}. \tag{10}$$

The indicator function $I(m \in j) = 1$ if event m is reconstructed in bin j, else $I(m \in j) = 0$. Figure 1(a) shows the distribution of $\boldsymbol{\nu}_{k=\mathrm{CTEQ5D}}$ in bins of the measured kinematic quantities. Figure 1(b) shows the distribution of the same events in the $\boldsymbol{\mu}_k$ binning.

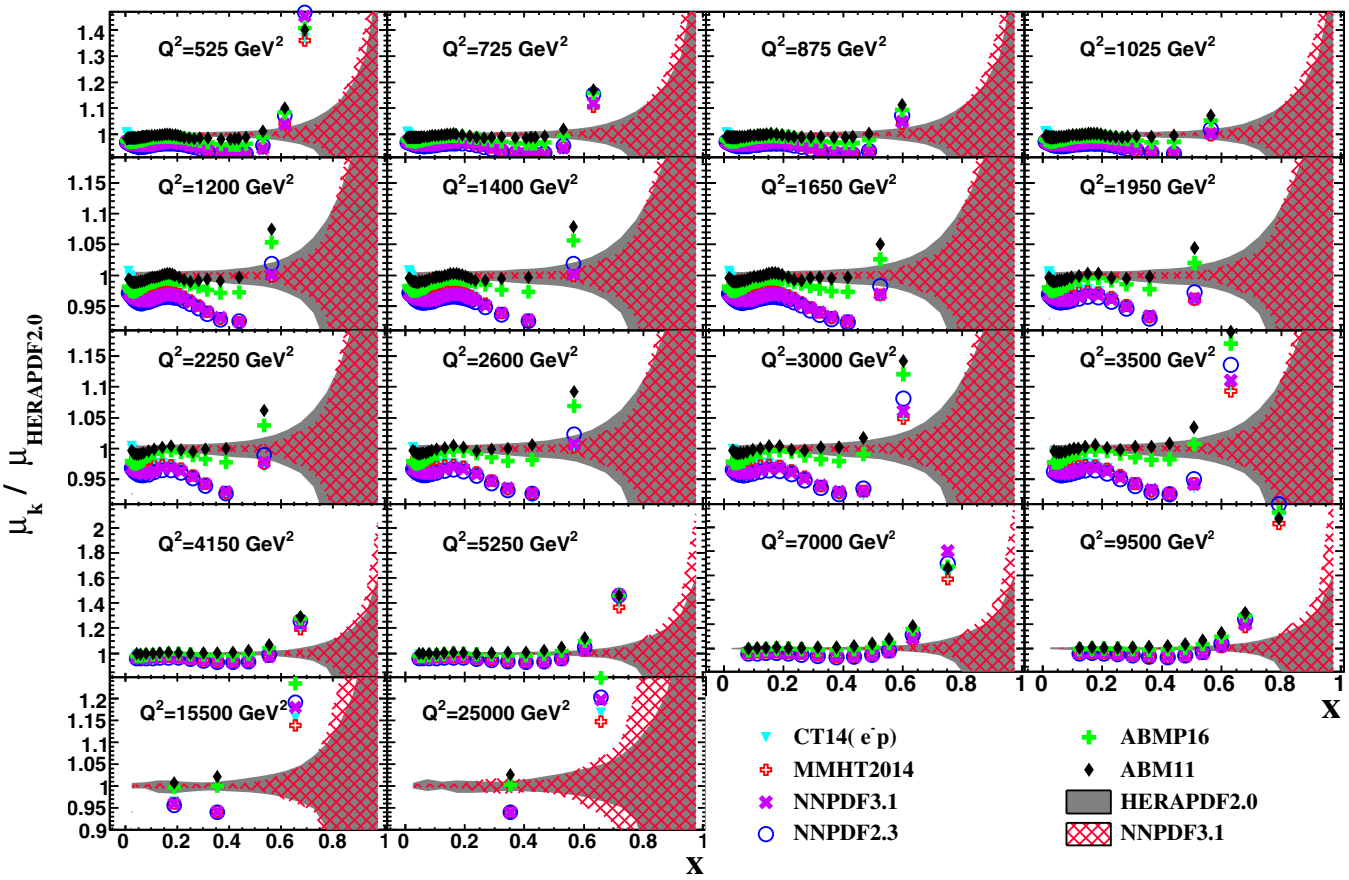

FIG. 2. Ratios of the elements of $\boldsymbol{\mu}_k$ for the PDF sets listed to those calculated using HERAPDF2.0 as functions of x in different Q^2 intervals for $e^- p$ data. The Q^2 value is given at the center of the bin, while the x value is at the mean x value of the events predicted in the bin for HERAPDF2.0. The shaded band represents the uncertainty quoted by HERAPDF2.0. The cross-hatched band represents the uncertainty quoted by NNPDF3.1.

IV. RESULTS

A. Comparison of predictions based on different PDF sets

Figures 2 and 3 show the ratios of the elements of $\boldsymbol{\mu}_k$ to the elements of $\boldsymbol{\mu}_{k=\mathrm{HERAPDF2.0}}$ as functions of x in different Q^2 intervals for selected PDF sets (CT14 [16], MMHT2014 [17], NNPDF3.1 [18], NNPDF2.3 [19], ABMP16 [20], and ABM11 [21]). The ratio is shown at the average x value from HERAPDF2.0 [9] in the bins.[2] The value of Q^2 is for the center of the respective bin. The expected number of events from the different PDF sets differ by more than a factor of 2 at large x values. There is also a systematic difference of several percent in the expectations at the smaller values of x among the different sets, which also predict different shapes as a function of x. The differences between the PDF predictions significantly exceed the 1 standard deviation uncertainties given by both HERAPDF2.0 and NNPDF3.1.

[2]The values of x were calculated for the MC sample from the four-vector of the exchanged boson and the proton.

B. Comparison of predictions to data

Figures 4 and 5 present a comparison of the number of events observed in data and the predictions from HERAPDF2.0 PDF for the $e^+ p$ and $e^- p$ data, respectively. The figures show that the data generally lie in the 68% range of expected results. However, for the $e^+ p$ data, the HERAPDF2.0-based predictions are on average 3.1% higher than the data while for the $e^- p$ data, the HERAPDF2.0-based predictions are on average 0.9% higher than the data. Figures similar to Figs. 4 and 5 are available in Supplemental Material [27] for the PDF sets ABMP16, AMB11, NNPDF3.1, NNPDF2.3, CT14, and MMHT2014.

The overall probabilities for the observed data sets given the expectations from the different PDF sets were calculated using Eq. (1). The natural logarithms of these probabilities are −538.3 and −581.5 for the $e^+ p$ and $e^- p$ data sets, respectively, for HERAPDF2.0. The corresponding p-values taking these probabilities as test statistics are 0.3 and 0.03. These probabilities account only for the statistical uncertainties. A summary of the results for different PDF sets is given in Table I. The table gives the ratio of the probabilities found for different PDF sets (P1) to

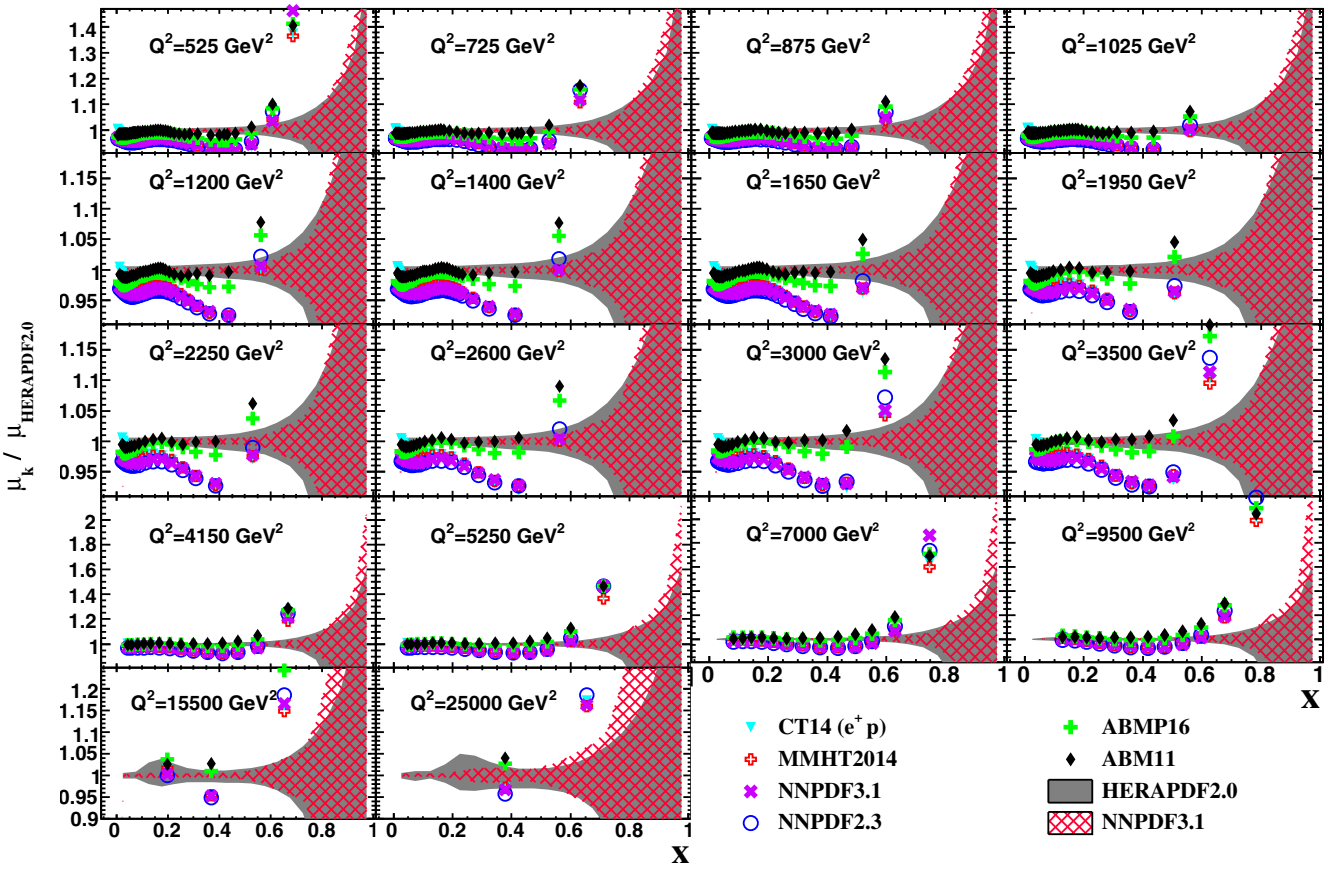

FIG. 3. Ratios of the elements of $\boldsymbol{\mu}_k$ for the PDF sets listed to those calculated using HERAPDF2.0 as functions of x in different Q^2 intervals for e^+p data. The Q^2 value is given at the center of the bin, while the x value is at the mean x value of the events predicted in the bin for HERAPDF2.0. The shaded band represents the uncertainty quoted by HERAPDF2.0. The cross-hatched band represents the uncertainty quoted by NNPDF3.1.

those found using HERAPDF2.0 (P2); see Eq. (2). In addition, the effective $\Delta\chi^2$ as defined in Eq. (2) is provided.

The predictions from all PDF sets yield p-values in an acceptable range for the e^+p data, indicating good overall agreement with the observed data. There are nevertheless significant differences in the probabilities. The highest probability for the e^+p data is found with the CT14 PDF set, with a Bayes factor of 5.9×10^5 relative to HERAPDF2.0, corresponding to $\Delta\chi^2 = -27$. For the e^-p data set, large differences are seen in the p-values, with only the HERAPDF2.0 and the ABM11 and ABMP16 sets yielding sizeable p-values. The Bayes factors vary by more than 6 orders of magnitude, resulting in $\Delta\chi^2$ values up to 31. The bin-by-bin comparison of the nominal predictions for the different PDF sets to the observations is given in Tables III and IV in Appendix A.

The probability evaluation was carried out in two x ranges: the "higher-x" range is defined as the three highest-x bins in each Q^2 range. The remaining x range is labeled "lower x." A substantial part of the data in the higher-x range has not been used in PDF extractions, while the data in the lower-x range have been included (albeit using different reconstruction techniques and coarser binning). The results for the different x ranges for both e^+p and e^-p data are given in Table II. There are significant differences in both x ranges. The predictions from the ABM11 and ABMP16 sets yield lower probabilities than HERAPDF2.0 in the lower-x range of the e^-p data, but higher probabilities in the higher-x range, while most of the difference in $\Delta\chi^2$ between CT14 and HERAPDF2.0 occurs in the higher-x range. For the e^+p data, similar values of $\Delta\chi^2$ are observed in both x ranges. These results indicate that the high-x data indeed have some discriminating power.

An effective statistical power of the higher-x data was estimated as follows. The normalization of the HERAPDF2.0 prediction was allowed to vary and an optimum was found using only the higher-x data. The change in the normalization resulting in a decrease of the logarithm of the likelihood of 0.5 was then determined. This normalization change was found to be small: 1.4% for the e^+p data and 1.2% for the e^-p data, indicating that these data should bring important new information.

All PDF sets provide not only nominal values for the parton distribution functions but also uncertainties that

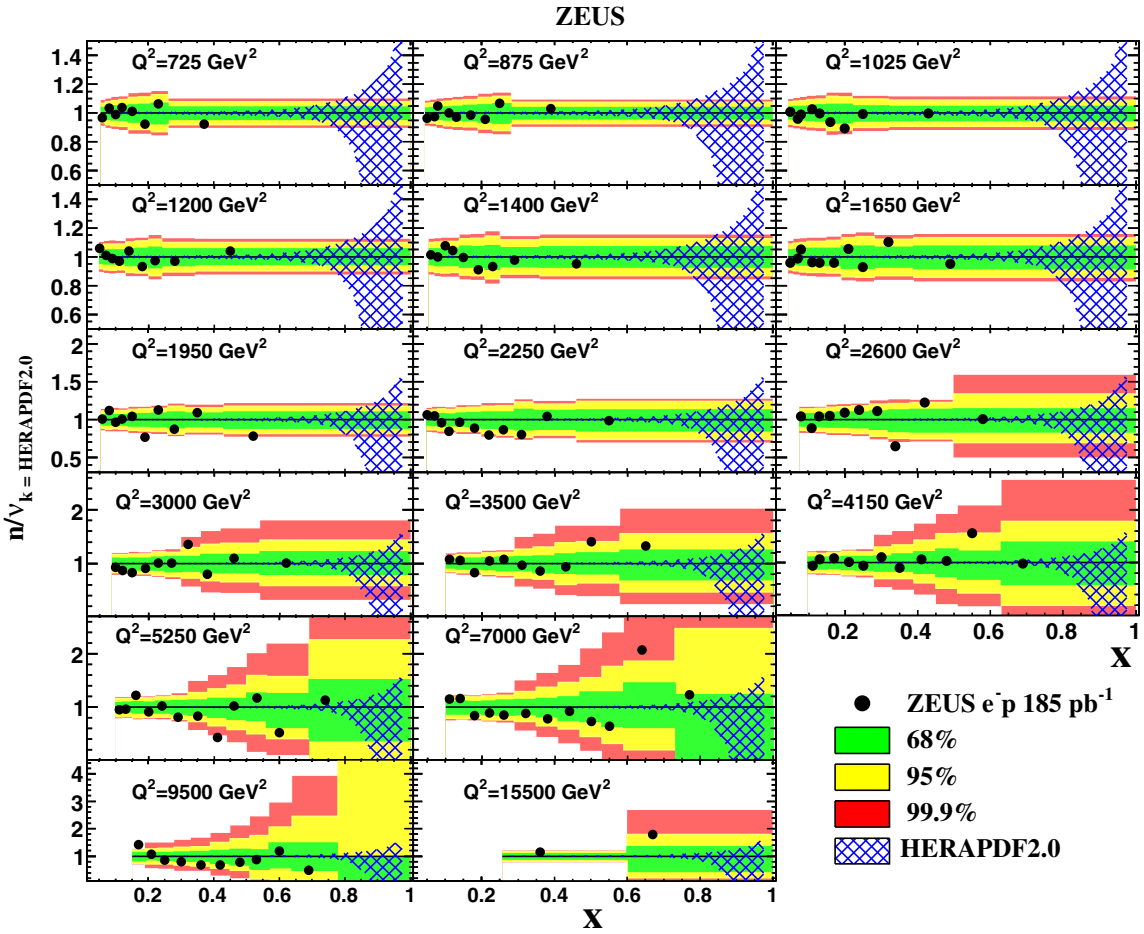

FIG. 4. Ratios of the number of observed events, $\boldsymbol{n}$, to the expectations from the HERAPDF2.0 set for $e^- p$ data. The points are plotted at the weighted average values of x. The green, yellow, and red bands give the smallest intervals [22] containing 68%, 95%, 99% probability, respectively. The ranges get wider as the number of expected events decreases. The cross-hatched band shows the uncertainty in the prediction associated with HERAPDF2.0.

translate into uncertainties on the predicted cross sections. The uncertainties for HERAPDF2.0 are provided as so-called variants; for all of these, predictions for the observed number of events were calculated. The resulting spread in the predictions is typically much smaller than the difference seen between predictions from different PDF sets as discussed above. The probabilities to observe the data for the different variants of HERAPDF2.0 were evaluated, with Bayes factors relative to the nominal predictions ranging from $0.4 \to 3$, the largest of this range corresponding to $\Delta\chi^2 \approx 2$. Given that the HERAPDF extraction uses a $\Delta\chi^2 = 1$ convention for evaluating uncertainties, a number of these variants would likely be excluded if the ZEUS high-x data were included in the PDF extraction.

V. SYSTEMATIC UNCERTAINTIES

In the discussion above, the nominal predictions from different PDF sets were used to predict event numbers, and a Poisson probability was calculated based on the observed number of events. This procedure accounts only for statistical uncertainties. In this section, the impact of systematic uncertainties on the probabilities is discussed. Two classes of systematic uncertainties can be distinguished—those that affect the predictions at the physics simulation level (the $\boldsymbol{\mu}$ and $\boldsymbol{R}$ values) and those that affect the matrix $\boldsymbol{T}$ accounting for detector and analysis effects. These are discussed separately for HERAPDF2.0.

For many of the PDF sets discussed in this paper, the combined H1 and ZEUS data [9] were included in their fitting procedure. A large fraction of the ZEUS neutral current data [23,24] entering the combination was taken during the same running period as the high-x data set considered here, and some of the systematic uncertainties are either identical to those discussed below or correlated to them. These uncertainties were already accounted for in the PDF extraction; i.e., the systematic uncertainties described below are not independent of the systematic uncertainties assigned to the PDF sets. A new PDF extraction would be necessary to account properly for the correlated systematic uncertainties. This point is discussed further below.

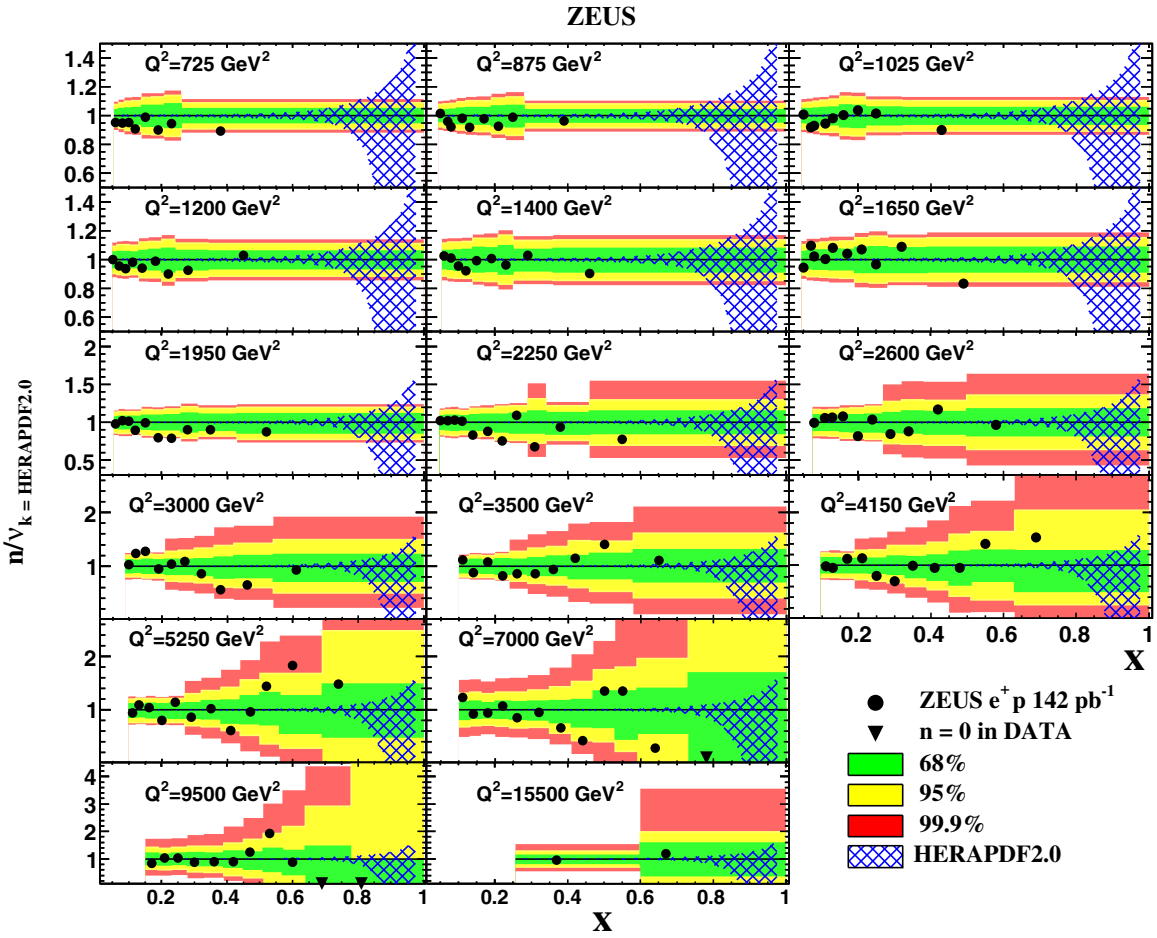

FIG. 5. Ratios of the number of observed events, $\boldsymbol{n}$, to the expectations from the HERAPDF2.0 set for e^+p data. The points are plotted at the weighted average values of x. The green, yellow, and red bands give the smallest intervals [22] containing 68%, 95%, 99% probability, respectively. The ranges get wider as the number of expected events decreases. The cross-hatched band shows the uncertainty in the prediction associated with HERAPDF2.0.

A. Uncertainties on μ and R

Possible systematic effects on the predictions are due to imperfect values of $\boldsymbol{R}$ and a small net polarization of the electron and positron beams. The latter effect was found to be negligible [8]. To test whether the diagonal matrix for $\boldsymbol{R}$ determined using the CTEQ5D PDF set was sufficiently accurate, the ratio of the generator-level predictions to the Born-level predictions was compared for different PDF sets for all bins used in the analysis. The ratios were found to be within the MC statistical uncertainties and typically well

TABLE I. The p-values, Bayes factors (P1/P2), and $\Delta\chi^2$ from comparisons of predictions using different NNLO PDF sets to the observed numbers of events. The Bayes factor is calculated relative to HERAPDF2.0, as is $\Delta\chi^2$. The results are shown separately for the e^-p and e^+p data sets.

	e^-p			e^+p		
PDF	p-value	P1/P2	$\Delta\chi^2$	p-value	P1/P2	$\Delta\chi^2$
HERAPDF2.0	2.8×10^{-2}	1.0	0.0	0.35	1.0	0.0
CT14	3.2×10^{-3}	7.6×10^{-3}	9.8	0.82	$5.9 \times 10^{+5}$	−27
MMHT2014	2.3×10^{-3}	2.1×10^{-3}	12	0.82	$4.7 \times 10^{+5}$	−26
NNPDF3.1	3.9×10^{-4}	3.2×10^{-6}	25	0.73	$9.0 \times 10^{+4}$	−23
NNPDF2.3	1.3×10^{-4}	2.3×10^{-7}	31	0.70	$4.2 \times 10^{+4}$	−21
ABMP16	2.6×10^{-2}	9.0×10^{-1}	0.21	0.64	$6.1 \times 10^{+2}$	−13
ABM11	3.3×10^{-2}	7.2×10^{-1}	0.67	0.45	2.8	−2.1

TABLE II. The Bayes factor (P1/P2) and $\Delta\chi^2$ (calculated relative to HERAPDF2.0) from comparisons of predictions using different NNLO PDF sets to the observed numbers of events are shown for two different x ranges. The higher-x region is defined as the highest three x bins in each Q^2 range. The remaining x range is labeled lower x.

	e^-p				e^+p			
	Lower x		Higher x		Lower x		Higher x	
PDF	P1/P2	$\Delta\chi^2$	P1/P2	$\Delta\chi^2$	P1/P2	$\Delta\chi^2$	P1/P2	$\Delta\chi^2$
HERAPDF2.0	1.0	0.0	1.0	0.0	1.0	0.0	1.0	0.0
CT14	6.0×10^{-1}	1.0	1.3×10^{-2}	8.7	$1.6\times10^{+3}$	−15	$3.6\times10^{+2}$	−12
MMHT2014	7.1×10^{-2}	5.3	2.9×10^{-2}	7.1	$1.3\times10^{+3}$	−14	$3.7\times10^{+2}$	−12
NNPDF3.1	9.1×10^{-5}	19	3.5×10^{-2}	6.7	$2.5\times10^{+2}$	−11	$3.6\times10^{+2}$	−12
NNPDF2.3	8.0×10^{-6}	23	2.9×10^{-2}	7.1	$1.2\times10^{+2}$	−9.5	$3.7\times10^{+2}$	−12
ABMP16	2.3×10^{-1}	3.0	4.0	−2.7	$4.8\times10^{+1}$	−7.8	$1.3\times10^{+1}$	−5.1
ABM11	2.3×10^{-1}	3.0	3.2	−2.3	4.2	−2.9	6.7×10^{-1}	0.8

within 1%. No systematic trends were observed. Variations in the Born-level cross sections are therefore not expected to produce significant uncertainties in the determination of $\boldsymbol{R}$. Limitations could still be present due to missing effects in the MC simulations used in this analysis. Should an improved simulation of radiative effects become available, the $\boldsymbol{R}$ matrix should be reevaluated and implemented.

The primary source of systematic uncertainty affecting $\boldsymbol{\mu}_k$ is the luminosity uncertainty, which acts as a scale factor on the elements of $\boldsymbol{\mu}_k$. The effect of the luminosity uncertainty was evaluated by increasing and decreasing $\boldsymbol{\mu}_k$ by $\pm1.8\%$, the luminosity uncertainty of the data set [8], separately for the e^+p and e^-p predictions, and recalculating the probabilities. The results are shown in Table V in Appendix B.

For e^-p data, an upward shift of the luminosity improved the agreement between predictions from the CT14, MMHT2014, NNPDF2.3, and NNPDF3.1 sets and the data, while worsening the agreement for HERAPDF2.0 and the ABM11 and ABMP16 sets. The negative shift gave lower (for the CT14, MMHT2014 and NNPDF2.3 and NNPDF3.1 much lower) probabilities. For HERAPDF2.0, the probability was not significantly changed.

For the e^+p data, the positive normalization shift made small changes for the CT14, MMHT2014, NNPDF2.3, and NNPDF3.1 sets and resulted in significantly worse probabilities for the HERAPDF2.0 and the ABM11 and ABMP16 sets. For the negative shift, the probability was significantly improved for HERAPDF2.0 and the ABM11 and ABMP16 sets while it generally became worse for the other PDF sets. Given that the normalization uncertainty is related to the data, it cannot be applied separately for the different PDFs sets. This implies that the significant difference in the predictions of the PDFs is not resolved by a change in the normalizations and no clear preference is seen for a given PDF set based strictly on the normalization of the data.

B. Uncertainties on $\boldsymbol{T}$

One source of uncertainty on $\boldsymbol{T}$ is the loss of information due to the finite bin sizes in the kinematic variables. A related source of uncertainty derives from using the same matrix for all PDF sets. To test the first effect, the bin sizes at the generator and Born level were systematically decreased until no further significant changes were observed in the predictions. Both effects were then evaluated by replacing the matrix procedure with an event-by-event reweighting procedure. The values of $\boldsymbol{\nu}_k$ were evaluated in this method as

$$\nu_{j,k} = \sum_m \frac{\frac{d^2\sigma(x,Q^2|\mathrm{PDF}_k)}{dxdQ^2}}{\frac{d^2\sigma(x,Q^2|\mathrm{CTEQ5D})}{dxdQ^2}} \omega_m^{\mathrm{MC}} \omega_m^{\mathrm{sim}} I(m \in j). \quad (11)$$

The sum runs over all generated MC events. The indicator function is used to select events reconstructed in bin j; the ratio of differential cross sections is evaluated using the Born-level differential cross sections calculated from the kinematic quantities at the generator level. The numerator is the differential cross section for a desired PDF set k, while the denominator is the differential cross section from the CTEQ5D PDF set. It was verified that the results are effectively identical for the different PDF sets considered in this paper. The differences in $\boldsymbol{\nu}_k$ were typically at the level of $< 0.1\%$ with a maximum difference of 1% seen in the highest-x and highest-Q^2 bins.

The limited size of the MC sample resulted in an uncertainty on $\boldsymbol{T}$. The statistical uncertainties on individual matrix elements are typically $\ll 1\%$, ranging to 1% in the highest-Q^2 and highest-x bins. Propagating these uncertainties to the entries in $\boldsymbol{\nu}_k$ results in negligible statistical uncertainties in the predicted numbers of events.

The variation in $\boldsymbol{T}$ from the dominant sources of uncertainty given in the ZEUS analysis [8] was further investigated. For each systematic effect considered, $\boldsymbol{T}$ was reevaluated and used to produce a new set of predictions for

the number of reconstructed events in the cross section bins. The probabilities can change by up to a factor 10, corresponding to effective χ^2 changes of almost five units. Although these changes are considerably smaller than those resulting from a change in the normalization, they should clearly be included in any new PDF extraction.

VI. PRESCRIPTION FOR PDF EXTRACTIONS INCLUDING THE HIGH-x DATA

Combining the ZEUS high-x data with other HERA data in the extraction of PDFs will require some care. The details will depend on the procedure, the emphasis of the study, and whether the high-x data are used in addition to the combined HERA data [9] or as a substitute for a part of the ZEUS data in a PDF extraction using individual ZEUS and H1 data sets. The latter ansatz could be used to answer the question whether and how the extended x range and the finer binning of the high-x data [8] impact the high-x part of the PDFs. For the HERA II data with $\sqrt{s} = 318$ GeV, the full set of H1 e^+ and e^- neutral current data [25] could be used together with the standard ZEUS neutral current data [23,24] for $Q^2 < 650$ GeV^2 and the ZEUS high-x data [8] for $Q^2 \geq 650$ GeV^2. The standard and high-x ZEUS data have a completely correlated normalization uncertainty while most of the remaining systematic uncertainties can be considered uncorrelated, since the reconstruction methods were significantly different. If wanted, the individual HERA II data sets could be augmented with the combined HERA I data [26] and HERA II combined data sets for lower $\sqrt{s}$. However, these data are not expected to have a large impact on the high-x part of the PDFs.

The use of the high-x data in addition to the combined HERA data [9] may however be preferred, since this permits a coherent treatment of systematic uncertainties over as much of the phase space as possible. Care has to be taken to avoid double counting by ensuring that bins individually added do not overlap with the bins from the remaining combined data. Table VI in Appendix C provides one possible selection. Combined e^+ and e^- data [9] for $x = 0.4$ and $x = 0.6$ were removed for Q^2 values at which ZEUS data [23,24] contributed. The finer binned ZEUS high-x data including the integrated bins were added as also listed in Table VI. The individual e^+ and e^- H1 data points [25] for the x and Q^2 values of the removed combined data points should also be added back individually.

For the procedure using combined and individual data, the normalizations of the individual data sets have to be adjusted. During the combination of H1 and ZEUS data sets, the normalizations of all individual data sets were shifted [9]. The normalization shifts of the ZEUS e^+ and e^- data sets as applied in the combination have to be applied to the individual ZEUS NC high-x e^+ and e^- data sets. This implies a *reduction* in the luminosity by the factors given in Table VII for these data sets. For the individual NC e^+ and e^- H1 data points [25] to be reintroduced in the analysis, the cross sections have to be increased by the factors given in Table VII. The normalization uncertainties quoted for the individual data sets should be treated as correlated systematic uncertainties on the individual ZEUS and H1 data points. The remaining systematic uncertainties should be treated as uncorrelated due to the different reconstruction techniques.

Different selections from the choices as listed in Table VI are conceivable. Parametrizations with sufficient flexibility in the high-x region could benefit from a more extended use of the high-x data. In any case, the procedures using Poisson statistics as outlined in this paper should be employed to make the optimal use of the high-x data.

VII. CONCLUSIONS

The ZEUS high-x data are unique and, to-date, have not been used in the extraction of proton parton distribution functions. They should be included in future PDF extractions using the matrix approach described in this paper. This data set will give access to a previously unused kinematic region, and will help constrain the large uncertainties on the partonic structure at the highest values of x.

The comparison of predictions from modern PDF sets in the kinematic range covered by the ZEUS high-x data shows large differences that are well beyond the uncertainties associated with the predictions, indicating that the uncertainties on the PDFs are underestimated. At the highest values of x, they could be significantly larger than currently thought, making the usage of high-x data even more important. The quantitative effect of the ZEUS high-x data on reducing the uncertainties is difficult to ascertain without carrying out the PDF extraction procedure in full detail. A proposal for including these data in future PDF extractions has been outlined.

ACKNOWLEDGMENTS

We appreciate the contributions to the construction, maintenance, and operation of the ZEUS detector of many people who are not listed as authors. The HERA machine group and the DESY computing staff are especially acknowledged for their success in providing excellent operation of the collider and the data-analysis environment. We thank the DESY directorate for their strong support and encouragement. The work is supported by the Italian National Institute for Nuclear Physics (INFN), the German Federal Ministry for Education and Research (BMBF), under Contract No. 05 H09PDF, High Impact Research (HIR) Grant No. UM.C/625/1/HIR/149 and University of Malaya Research Grant (UMRG) Grants No. RU006-2013, No. RP012A-13AFR, and No. RP012B-13AFR from Universiti Malaya, and Exploratory Research Grant Scheme (ERGS) Grant No. ER004-2012A from the Ministry of Education, Malaysia, the Polish National Science Centre (NCN)

Grant No. DEC-2014/13/B/ST2/02486, the Science and Technology Facilities Council, United Kingdom, the German Federal Ministry for Education and Research (BMBF), under Contract No. 05h09GUF, and the SFB 676 of the Deutsche Forschungsgemeinschaft (DFG), the Japanese Ministry of Education, Culture, Sports, Science and Technology (MEXT) and its grants for Scientific Research, the Israel Science Foundation, in part by the Office of Nuclear Physics within the U.S. DOE Office of Science, the Natural Sciences and Engineering Research Council of Canada (NSERC), and by DESY.

APPENDIX A: TABLES OF DATA AND PDF PREDICTIONS

TABLE III. The comparison of event counts in data and in MC for the $e^- p$ sample, using different PDFs. The first two columns of the table contain the Q^2 and x values for the center of the bin and the third column contains the number of events reconstructed in the bin in data ($\boldsymbol{n}$). The further columns contain expectations ($\boldsymbol{\nu}$) and the probability $P(\boldsymbol{n}|\boldsymbol{\nu})$ for the PDFs discussed in the paper.

Q^2		Data	HERAPDF2.0		CT14		MMHT2014		NNPDF3.1		NNPDF2.3		ABMP16		AMB11	
(GeV^2)	x	$\boldsymbol{n}$	$\boldsymbol{\nu}$	$P(\boldsymbol{n}\|\boldsymbol{\nu})$	$\boldsymbol{\nu}$	$P(\boldsymbol{n}\|\boldsymbol{\nu})$	$\boldsymbol{\nu}$	$P(\boldsymbol{n}\|\boldsymbol{\nu})$	$\boldsymbol{\nu}$	$P(\boldsymbol{n}\|\boldsymbol{\nu})$	$\boldsymbol{\nu}$	$P(\boldsymbol{n}\|\boldsymbol{\nu})$	$\boldsymbol{\nu}$	$P(\boldsymbol{n}\|\boldsymbol{\nu})$	$\boldsymbol{\nu}$	$P(\boldsymbol{n}\|\boldsymbol{\nu})$
725	0.06	743	768.1	0.010	751.6	0.014	747.6	0.014	736.2	0.014	732.5	0.014	750.0	0.014	759.3	0.012
725	0.08	580	560.9	0.012	547.2	0.006	545.1	0.006	537.1	0.003	535.0	0.003	549.7	0.007	555.6	0.010
725	0.10	441	445.0	0.019	433.7	0.018	432.3	0.017	426.6	0.015	425.3	0.014	438.0	0.019	442.0	0.019
725	0.12	416	401.2	0.015	391.0	0.009	390.0	0.008	385.9	0.006	384.7	0.006	396.1	0.012	399.4	0.014
725	0.16	283	279.9	0.023	273.0	0.020	272.3	0.019	270.3	0.018	269.3	0.017	277.1	0.022	279.4	0.023
725	0.19	248	268.4	0.011	261.4	0.018	260.9	0.018	259.4	0.020	258.4	0.021	265.7	0.014	267.9	0.012
725	0.23	227	213.3	0.017	206.7	0.010	206.5	0.010	205.5	0.009	204.8	0.008	210.7	0.014	212.0	0.016
725	0.63	504	545.5	0.004	516.1	0.015	517.8	0.015	517.2	0.015	516.5	0.015	535.0	0.007	542.5	0.004
875	0.05	789	819.2	0.008	803.9	0.012	798.3	0.013	786.5	0.014	782.7	0.014	798.9	0.013	809.2	0.011
875	0.07	681	699.0	0.012	683.2	0.015	680.0	0.015	669.9	0.014	666.8	0.013	683.8	0.015	691.7	0.014
875	0.09	604	576.5	0.009	562.2	0.004	560.2	0.003	552.3	0.002	550.5	0.001	566.4	0.005	571.9	0.007
875	0.11	493	492.8	0.018	480.2	0.015	478.8	0.015	473.1	0.012	471.8	0.011	486.1	0.017	490.3	0.018
875	0.14	403	415.8	0.016	405.4	0.020	404.4	0.020	400.7	0.020	399.5	0.020	411.4	0.018	414.5	0.017
875	0.17	385	391.1	0.019	381.4	0.020	380.5	0.020	378.2	0.019	376.7	0.019	387.8	0.020	390.9	0.019
875	0.21	271	283.8	0.018	275.9	0.023	275.5	0.023	274.2	0.024	273.1	0.024	281.1	0.020	283.0	0.019
875	0.26	258	241.9	0.015	233.4	0.007	233.3	0.007	232.4	0.006	231.6	0.006	238.7	0.012	240.0	0.013
875	0.64	671	650.3	0.011	613.2	0.001	615.5	0.001	615.3	0.001	614.7	0.001	638.3	0.007	648.5	0.011
1025	0.05	598	593.3	0.016	582.4	0.013	578.3	0.012	569.9	0.008	567.3	0.007	578.9	0.012	586.4	0.015
1025	0.07	489	508.8	0.012	497.4	0.017	495.0	0.017	487.8	0.018	485.7	0.018	497.9	0.017	503.7	0.015
1025	0.09	450	454.2	0.018	443.0	0.018	441.4	0.017	435.3	0.015	434.0	0.014	446.5	0.018	450.7	0.019
1025	0.11	402	391.5	0.017	381.6	0.012	380.5	0.011	376.0	0.008	375.1	0.008	386.5	0.015	389.7	0.016
1025	0.14	342	343.3	0.021	334.8	0.020	333.9	0.020	331.0	0.018	330.0	0.017	340.0	0.021	342.5	0.022
1025	0.16	231	245.9	0.017	239.9	0.022	239.3	0.023	237.9	0.024	237.0	0.024	244.1	0.018	246.0	0.017
1025	0.20	224	250.7	0.006	244.0	0.011	243.6	0.012	242.4	0.013	241.4	0.014	248.6	0.007	250.4	0.006
1025	0.27	363	365.9	0.021	352.2	0.018	352.1	0.018	350.8	0.017	349.6	0.016	361.0	0.021	363.2	0.021
1025	0.66	414	415.6	0.019	390.5	0.010	392.4	0.011	392.6	0.011	392.5	0.011	408.7	0.019	416.2	0.019
1200	0.06	552	522.2	0.007	512.1	0.004	508.8	0.003	501.5	0.002	499.2	0.001	510.1	0.003	516.6	0.005
1200	0.07	454	449.4	0.018	439.1	0.015	437.0	0.013	430.9	0.010	429.2	0.009	440.3	0.015	445.2	0.017
1200	0.09	412	416.5	0.019	406.2	0.019	404.7	0.018	399.4	0.016	398.3	0.016	410.0	0.020	413.7	0.020
1200	0.12	430	443.3	0.016	432.3	0.019	430.9	0.019	426.3	0.019	425.2	0.019	438.3	0.018	441.7	0.017
1200	0.15	326	313.6	0.017	306.0	0.012	305.1	0.011	302.9	0.009	301.9	0.009	311.1	0.015	313.3	0.017
1200	0.18	272	291.2	0.013	283.9	0.019	283.2	0.019	281.8	0.020	280.6	0.021	289.1	0.014	291.4	0.013
1200	0.22	209	214.8	0.025	208.4	0.028	208.1	0.028	207.3	0.027	206.5	0.027	212.9	0.027	214.1	0.026
1200	0.29	310	319.7	0.019	305.9	0.022	306.0	0.022	305.1	0.022	304.1	0.021	314.8	0.022	317.2	0.021
1200	0.67	368	354.0	0.016	332.3	0.003	334.0	0.004	334.3	0.004	334.5	0.004	349.1	0.013	356.0	0.017
1400	0.06	358	353.1	0.020	345.7	0.017	343.7	0.016	338.9	0.012	337.4	0.011	345.4	0.017	349.6	0.019
1400	0.08	308	308.8	0.023	301.5	0.021	300.1	0.021	296.1	0.018	295.1	0.017	303.3	0.022	306.3	0.023
1400	0.10	317	294.6	0.010	287.3	0.005	286.2	0.004	282.8	0.003	282.1	0.003	290.7	0.007	293.1	0.009
1400	0.12	300	287.4	0.018	280.3	0.012	279.4	0.011	276.9	0.009	276.1	0.008	284.6	0.015	286.7	0.017

(Table continued)

TABLE III. *(Continued)*

Q^2		Data	HERAPDF2.0		CT14		MMHT2014		NNPDF3.1		NNPDF2.3		ABMP16		AMB11	
(GeV^2)	x	n	ν	$P(n\|\nu)$	ν	$P(n\|\nu)$	ν	$P(n\|\nu)$	ν	$P(n\|\nu)$	ν	$P(n\|\nu)$	ν	$P(n\|\nu)$	ν	$P(n\|\nu)$
1400	0.16	206	207.1	0.028	202.1	0.027	201.6	0.026	200.3	0.026	199.6	0.025	205.7	0.028	207.2	0.028
1400	0.19	183	201.1	0.013	195.8	0.019	195.4	0.020	194.6	0.021	193.8	0.022	199.8	0.014	201.2	0.013
1400	0.23	139	148.8	0.024	144.1	0.031	143.9	0.031	143.3	0.032	142.8	0.032	147.5	0.026	148.2	0.025
1400	0.30	231	236.5	0.025	225.3	0.024	225.5	0.025	225.0	0.024	224.2	0.024	232.7	0.026	234.9	0.025
1400	0.68	202	212.4	0.022	199.4	0.028	200.5	0.028	200.8	0.028	201.0	0.028	210.2	0.024	214.6	0.019
1650	0.05	419	437.9	0.013	430.1	0.017	426.8	0.018	421.1	0.019	419.3	0.019	427.8	0.018	433.5	0.015
1650	0.07	358	362.2	0.021	354.3	0.021	352.4	0.020	347.6	0.018	346.3	0.017	354.9	0.021	359.1	0.021
1650	0.09	351	334.4	0.014	326.3	0.009	324.9	0.008	320.7	0.005	319.9	0.005	329.1	0.010	332.2	0.013
1650	0.11	298	310.2	0.018	302.6	0.022	301.4	0.023	298.2	0.023	297.5	0.023	306.7	0.020	309.1	0.019
1650	0.14	276	288.2	0.018	281.3	0.023	280.4	0.023	278.2	0.024	277.4	0.024	286.0	0.020	288.0	0.019
1650	0.17	254	265.0	0.020	258.6	0.024	257.9	0.024	256.6	0.025	255.6	0.025	263.6	0.021	265.5	0.019
1650	0.21	195	184.6	0.021	179.3	0.015	179.0	0.014	178.3	0.013	177.6	0.013	183.4	0.020	184.5	0.021
1650	0.26	158	170.3	0.020	163.9	0.029	163.9	0.029	163.3	0.029	162.8	0.030	168.5	0.023	169.4	0.021
1650	0.34	227	205.7	0.009	194.2	0.002	194.6	0.002	194.4	0.002	193.7	0.002	201.8	0.006	204.5	0.008
1650	0.70	173	181.9	0.024	170.9	0.030	171.9	0.030	172.2	0.030	172.7	0.030	180.9	0.025	184.9	0.021
1950	0.06	265	262.5	0.024	257.1	0.022	255.4	0.021	252.1	0.018	251.1	0.017	257.0	0.022	260.2	0.024
1950	0.08	251	224.0	0.005	218.7	0.003	217.6	0.002	214.9	0.001	214.2	0.001	220.1	0.003	222.4	0.004
1950	0.10	214	221.5	0.024	216.1	0.027	215.1	0.027	212.7	0.027	212.2	0.027	218.7	0.026	220.6	0.025
1950	0.12	228	226.8	0.026	221.3	0.024	220.6	0.023	218.7	0.022	218.1	0.021	224.9	0.026	226.5	0.026
1950	0.16	172	164.7	0.026	160.7	0.021	160.2	0.020	159.3	0.019	158.7	0.018	163.8	0.025	164.9	0.026
1950	0.19	124	161.6	0.000	157.3	0.001	157.0	0.001	156.3	0.001	155.7	0.001	160.8	0.000	161.9	0.000
1950	0.23	157	139.5	0.011	134.8	0.006	134.7	0.006	134.2	0.005	133.8	0.005	138.4	0.010	139.1	0.011
1950	0.29	86	98.5	0.019	94.0	0.030	94.1	0.030	93.9	0.031	93.6	0.031	97.2	0.022	98.0	0.020
1950	0.37	138	126.5	0.020	118.3	0.007	118.8	0.008	118.8	0.008	118.4	0.007	123.9	0.016	126.1	0.020
1950	0.72	74	94.7	0.004	89.6	0.011	90.1	0.010	90.2	0.010	90.7	0.009	95.1	0.004	97.3	0.002
2250	0.06	214	200.9	0.018	197.1	0.013	195.6	0.012	193.1	0.009	192.3	0.008	196.5	0.013	199.1	0.016
2250	0.07	187	178.5	0.024	174.4	0.019	173.4	0.017	171.2	0.014	170.7	0.014	175.1	0.020	177.1	0.022
2250	0.09	153	159.9	0.028	156.0	0.031	155.3	0.032	153.5	0.032	153.1	0.032	157.6	0.030	159.1	0.029
2250	0.12	159	187.6	0.003	183.1	0.006	182.3	0.007	180.6	0.008	180.2	0.009	185.8	0.004	187.2	0.003
2250	0.15	132	137.1	0.032	133.8	0.034	133.4	0.035	132.5	0.035	132.1	0.035	136.3	0.032	137.2	0.031
2250	0.18	117	132.0	0.015	128.7	0.021	128.3	0.022	127.8	0.023	127.2	0.024	131.4	0.016	132.4	0.015
2250	0.22	75	94.6	0.005	91.7	0.009	91.6	0.009	91.2	0.010	90.9	0.011	94.0	0.006	94.6	0.005
2250	0.27	72	82.9	0.022	79.5	0.033	79.6	0.032	79.3	0.033	79.0	0.034	82.1	0.025	82.6	0.023
2250	0.32	48	60.0	0.016	56.8	0.028	56.9	0.028	56.8	0.028	56.6	0.029	59.1	0.019	59.8	0.016
2250	0.40	76	73.1	0.043	68.0	0.029	68.3	0.030	68.4	0.030	68.2	0.030	71.7	0.040	73.1	0.043
2250	0.73	51	51.7	0.056	49.3	0.054	49.5	0.055	49.6	0.055	50.0	0.055	52.4	0.055	53.6	0.052
2600	0.09	168	161.4	0.027	157.5	0.022	156.7	0.021	154.9	0.018	154.5	0.017	158.9	0.024	160.5	0.026
2600	0.11	142	159.8	0.012	155.9	0.018	155.2	0.019	153.7	0.021	153.3	0.022	158.1	0.014	159.4	0.013
2600	0.14	160	153.8	0.028	150.1	0.023	149.5	0.022	148.5	0.020	148.0	0.020	152.7	0.027	153.8	0.028
2600	0.16	119	113.3	0.032	110.6	0.027	110.2	0.026	109.7	0.025	109.3	0.024	112.9	0.031	113.7	0.032
2600	0.20	122	112.1	0.024	109.0	0.017	108.8	0.017	108.4	0.016	107.9	0.015	111.6	0.023	112.3	0.024
2600	0.24	111	98.3	0.017	94.7	0.010	94.7	0.010	94.4	0.009	94.0	0.009	97.6	0.016	98.1	0.017
2600	0.30	74	66.4	0.030	63.1	0.019	63.2	0.019	63.1	0.019	62.9	0.018	65.5	0.028	66.2	0.030
2600	0.35	37	57.0	0.001	53.3	0.004	53.5	0.004	53.5	0.004	53.3	0.004	55.9	0.002	56.9	0.001
2600	0.44	67	54.7	0.013	50.7	0.004	51.0	0.005	51.1	0.005	51.0	0.005	53.8	0.011	55.0	0.014
2600	0.75	36	35.9	0.066	34.7	0.065	34.8	0.065	34.9	0.065	35.3	0.066	37.0	0.066	37.8	0.063
3000	0.10	104	112.7	0.028	109.9	0.033	109.3	0.034	108.2	0.036	108.0	0.036	111.3	0.031	112.3	0.029
3000	0.12	106	122.1	0.013	119.1	0.018	118.6	0.019	117.7	0.021	117.4	0.022	121.1	0.014	122.0	0.013
3000	0.16	77	92.8	0.011	90.5	0.016	90.2	0.016	89.8	0.017	89.5	0.018	92.4	0.012	93.1	0.010
3000	0.19	82	90.9	0.028	88.5	0.035	88.3	0.035	87.9	0.036	87.6	0.037	90.6	0.029	91.2	0.027
3000	0.23	68	67.3	0.048	65.0	0.045	65.0	0.045	64.7	0.045	64.5	0.044	66.9	0.048	67.2	0.048
3000	0.28	58	57.8	0.052	55.3	0.049	55.3	0.049	55.2	0.049	55.0	0.048	57.3	0.052	57.7	0.052

(Table continued)

TABLE III. *(Continued)*

Q^2		Data	HERAPDF2.0		CT14		MMHT2014		NNPDF3.1		NNPDF2.3		ABMP16		AMB11	
(GeV^2)	x	n	ν	$P(n\|\nu)$	ν	$P(n\|\nu)$	ν	$P(n\|\nu)$	ν	$P(n\|\nu)$	ν	$P(n\|\nu)$	ν	$P(n\|\nu)$	ν	$P(n\|\nu)$
3000	0.33	65	48.0	0.003	45.2	0.001	45.3	0.001	45.3	0.001	45.1	0.001	47.3	0.003	48.0	0.003
3000	0.39	26	32.5	0.039	30.1	0.058	30.3	0.057	30.4	0.056	30.2	0.057	31.9	0.044	32.5	0.038
3000	0.48	32	29.1	0.061	26.9	0.045	27.1	0.046	27.1	0.046	27.1	0.047	28.7	0.059	29.4	0.063
3000	0.77	19	18.9	0.091	18.6	0.091	18.7	0.091	18.8	0.091	19.0	0.091	19.9	0.089	20.3	0.087
3500	0.12	151	140.1	0.021	136.7	0.016	136.0	0.015	134.9	0.013	134.6	0.012	138.8	0.019	140.0	0.021
3500	0.15	117	111.3	0.032	108.6	0.027	108.2	0.026	107.6	0.025	107.2	0.024	110.8	0.031	111.6	0.032
3500	0.18	90	109.4	0.007	106.5	0.011	106.2	0.011	105.9	0.012	105.4	0.013	109.0	0.007	109.8	0.006
3500	0.22	84	80.1	0.040	77.5	0.034	77.5	0.033	77.2	0.033	76.9	0.032	79.8	0.039	80.2	0.040
3500	0.27	76	70.8	0.038	67.8	0.028	67.8	0.028	67.6	0.028	67.4	0.027	70.2	0.036	70.7	0.038
3500	0.32	48	49.6	0.056	46.8	0.057	46.9	0.057	46.9	0.057	46.7	0.057	48.9	0.057	49.6	0.056
3500	0.37	34	39.8	0.044	37.0	0.060	37.2	0.059	37.2	0.059	37.1	0.060	39.1	0.048	39.9	0.043
3500	0.43	23	24.6	0.079	22.7	0.083	22.9	0.083	22.9	0.083	22.9	0.083	24.2	0.080	24.8	0.078
3500	0.52	33	23.5	0.013	21.9	0.006	22.1	0.007	22.1	0.007	22.2	0.007	23.5	0.013	24.1	0.016
3500	0.79	17	12.8	0.052	13.0	0.056	13.0	0.056	13.1	0.057	13.3	0.060	13.9	0.070	14.2	0.074
4150	0.11	90	95.3	0.036	93.0	0.040	92.4	0.041	91.7	0.041	91.5	0.042	94.3	0.038	95.2	0.036
4150	0.14	98	92.7	0.035	90.4	0.029	90.0	0.029	89.5	0.027	89.2	0.026	92.1	0.034	92.8	0.035
4150	0.17	103	95.5	0.030	93.1	0.024	92.8	0.023	92.5	0.022	92.1	0.021	95.3	0.029	96.0	0.031
4150	0.21	69	68.5	0.048	66.4	0.046	66.3	0.045	66.1	0.045	65.8	0.044	68.3	0.048	68.7	0.048
4150	0.26	60	63.9	0.046	61.3	0.051	61.3	0.051	61.1	0.051	60.9	0.051	63.5	0.047	63.8	0.046
4150	0.31	47	42.6	0.047	40.3	0.034	40.4	0.035	40.4	0.035	40.2	0.034	42.2	0.044	42.7	0.047
4150	0.36	31	34.5	0.059	32.2	0.070	32.3	0.070	32.4	0.069	32.2	0.070	34.0	0.062	34.6	0.059
4150	0.42	24	22.5	0.077	20.8	0.064	20.9	0.066	21.0	0.066	20.9	0.065	22.2	0.075	22.7	0.078
4150	0.48	14	13.6	0.105	12.6	0.098	12.7	0.099	12.7	0.099	12.7	0.100	13.5	0.105	13.9	0.106
4150	0.57	18	11.6	0.020	11.0	0.015	11.1	0.015	11.1	0.015	11.2	0.016	11.8	0.024	12.2	0.028
4150	0.81	5	5.1	0.175	5.5	0.172	5.4	0.173	5.5	0.171	5.6	0.170	5.8	0.166	5.9	0.163
5250	0.11	114	120.0	0.032	116.9	0.036	116.1	0.037	115.3	0.037	115.1	0.037	118.6	0.034	119.9	0.032
5250	0.14	117	122.2	0.033	119.1	0.036	118.4	0.036	117.9	0.037	117.5	0.037	121.4	0.034	122.5	0.033
5250	0.16	117	95.7	0.004	93.2	0.002	92.8	0.002	92.5	0.002	92.1	0.002	95.4	0.004	96.2	0.004
5250	0.20	91	100.0	0.028	97.0	0.035	96.8	0.035	96.5	0.035	96.1	0.036	99.8	0.028	100.4	0.026
5250	0.24	92	90.0	0.041	86.5	0.035	86.5	0.035	86.3	0.035	86.0	0.034	89.6	0.040	90.1	0.041
5250	0.30	52	64.3	0.016	60.9	0.028	61.1	0.027	61.0	0.028	60.8	0.028	63.7	0.018	64.5	0.015
5250	0.35	42	50.2	0.030	46.9	0.047	47.1	0.046	47.2	0.046	47.0	0.047	49.6	0.033	50.5	0.029
5250	0.41	14	31.9	0.000	29.5	0.001	29.7	0.001	29.8	0.001	29.7	0.001	31.5	0.000	32.3	0.000
5250	0.47	21	20.6	0.086	19.0	0.078	19.1	0.080	19.2	0.080	19.2	0.080	20.4	0.086	21.0	0.087
5250	0.53	14	11.9	0.089	11.2	0.077	11.3	0.079	11.3	0.078	11.4	0.080	12.1	0.092	12.4	0.096
5250	0.62	5	9.6	0.047	9.5	0.048	9.5	0.048	9.5	0.047	9.7	0.043	10.2	0.034	10.5	0.029
5250	0.84	3	2.6	0.219	3.1	0.224	3.1	0.224	3.2	0.223	3.2	0.223	3.3	0.221	3.3	0.220
7000	0.12	93	81.0	0.018	78.9	0.013	78.2	0.011	77.9	0.010	77.7	0.010	80.1	0.015	81.1	0.018
7000	0.15	89	76.4	0.016	74.4	0.011	73.9	0.010	73.7	0.010	73.5	0.009	76.0	0.015	76.7	0.017
7000	0.18	68	80.8	0.017	78.5	0.023	78.2	0.024	78.0	0.025	77.7	0.026	80.6	0.017	81.3	0.015
7000	0.22	56	62.8	0.036	60.6	0.044	60.6	0.044	60.5	0.045	60.2	0.046	62.7	0.037	63.1	0.035
7000	0.27	49	57.5	0.029	54.9	0.041	55.0	0.041	54.8	0.041	54.6	0.042	57.2	0.031	57.6	0.029
7000	0.32	41	46.5	0.044	43.7	0.057	43.9	0.056	43.9	0.057	43.7	0.057	46.0	0.047	46.8	0.043
7000	0.38	23	29.2	0.041	27.1	0.060	27.3	0.058	27.3	0.058	27.2	0.059	28.9	0.044	29.5	0.038
7000	0.44	17	18.5	0.091	17.1	0.096	17.2	0.096	17.2	0.096	17.2	0.096	18.3	0.092	18.8	0.088
7000	0.50	8	11.0	0.090	10.2	0.108	10.3	0.106	10.3	0.106	10.3	0.105	11.0	0.088	11.3	0.081
7000	0.56	4	6.2	0.123	6.0	0.134	6.0	0.133	6.0	0.133	6.1	0.130	6.5	0.113	6.7	0.105
7000	0.66	10	4.8	0.015	5.1	0.019	5.0	0.019	5.0	0.019	5.2	0.022	5.4	0.027	5.5	0.030
7000	0.86	1	0.8	0.360	1.1	0.367	1.1	0.367	1.1	0.365	1.1	0.366	1.1	0.365	1.1	0.365
9500	0.17	76	53.7	0.001	52.1	0.000	51.8	0.000	51.8	0.000	51.6	0.000	53.5	0.001	54.1	0.001
9500	0.21	53	49.5	0.049	47.9	0.042	47.8	0.041	47.7	0.041	47.5	0.040	49.4	0.048	49.8	0.050

(Table continued)

TABLE III. *(Continued)*

Q^2		Data	HERAPDF2.0		CT14		MMHT2014		NNPDF3.1		NNPDF2.3		ABMP16		AMB11	
(GeV^2)	x	$\boldsymbol{n}$	$\boldsymbol{\nu}$	$P(\boldsymbol{n}\|\boldsymbol{\nu})$	$\boldsymbol{\nu}$	$P(\boldsymbol{n}\|\boldsymbol{\nu})$	$\boldsymbol{\nu}$	$P(\boldsymbol{n}\|\boldsymbol{\nu})$	$\boldsymbol{\nu}$	$P(\boldsymbol{n}\|\boldsymbol{\nu})$	$\boldsymbol{\nu}$	$P(\boldsymbol{n}\|\boldsymbol{\nu})$	$\boldsymbol{\nu}$	$P(\boldsymbol{n}\|\boldsymbol{\nu})$	$\boldsymbol{\nu}$	$P(\boldsymbol{n}\|\boldsymbol{\nu})$
9500	0.26	40	47.0	0.037	44.9	0.048	44.9	0.048	44.9	0.048	44.7	0.049	46.8	0.037	47.1	0.036
9500	0.31	27	34.0	0.035	32.1	0.050	32.2	0.049	32.2	0.049	32.1	0.050	33.8	0.036	34.3	0.033
9500	0.36	19	28.2	0.017	26.3	0.030	26.4	0.029	26.4	0.029	26.3	0.029	27.9	0.018	28.5	0.015
9500	0.42	12	17.4	0.044	16.1	0.065	16.2	0.063	16.2	0.063	16.2	0.063	17.3	0.046	17.7	0.040
9500	0.48	8	10.4	0.103	9.7	0.120	9.7	0.119	9.7	0.119	9.8	0.118	10.4	0.103	10.7	0.096
9500	0.54	5	5.7	0.168	5.4	0.173	5.4	0.172	5.4	0.172	5.5	0.172	5.8	0.165	6.0	0.160
9500	0.60	4	3.4	0.185	3.4	0.185	3.4	0.185	3.4	0.186	3.5	0.188	3.6	0.192	3.8	0.194
9500	0.71	1	2.0	0.265	2.3	0.230	2.3	0.234	2.3	0.229	2.4	0.221	2.5	0.210	2.5	0.204
9500	0.89	1	0.2	0.149	0.3	0.202	0.3	0.200	0.3	0.223	0.3	0.209	0.3	0.208	0.3	0.208
15500	0.43	120	103.8	0.011	97.7	0.003	98.0	0.004	98.0	0.004	97.9	0.004	103.8	0.011	105.8	0.015
15500	0.80	8	4.5	0.045	4.8	0.058	4.8	0.057	4.9	0.061	4.9	0.062	5.1	0.071	5.2	0.075

TABLE IV. The comparison of event counts in data and in MC for the e^+p sample, using different PDFs. The first two columns of the table contain the Q^2 and x values for the center of the bin and the third column contains the number of events reconstructed in the bin in data ($\boldsymbol{n}$). The further columns contain expectations ($\boldsymbol{\nu}$) and the probability $P(\boldsymbol{n}|\boldsymbol{\nu})$ for the PDFs discussed in the paper.

Q^2		Data	HERAPDF2.0		CT14		MMHT2014		NNPDF3.1		NNPDF2.3		ABMP16		AMB11	
(GeV^2)	x	$\boldsymbol{n}$	$\boldsymbol{\nu}$	$P(\boldsymbol{n}\|\boldsymbol{\nu})$	$\boldsymbol{\nu}$	$P(\boldsymbol{n}\|\boldsymbol{\nu})$	$\boldsymbol{\nu}$	$P(\boldsymbol{n}\|\boldsymbol{\nu})$	$\boldsymbol{\nu}$	$P(\boldsymbol{n}\|\boldsymbol{\nu})$	$\boldsymbol{\nu}$	$P(\boldsymbol{n}\|\boldsymbol{\nu})$	$\boldsymbol{\nu}$	$P(\boldsymbol{n}\|\boldsymbol{\nu})$	$\boldsymbol{\nu}$	$P(\boldsymbol{n}\|\boldsymbol{\nu})$
725	0.06	567	594.3	0.009	581.8	0.014	578.8	0.015	569.9	0.017	566.9	0.017	580.5	0.014	587.4	0.012
725	0.08	418	440.2	0.011	429.6	0.017	428.1	0.017	421.6	0.019	419.9	0.019	431.6	0.016	435.9	0.013
725	0.10	321	337.2	0.015	328.7	0.020	327.8	0.021	323.4	0.022	322.3	0.022	332.0	0.018	334.9	0.017
725	0.12	274	302.3	0.006	294.7	0.011	294.0	0.012	290.9	0.015	290.0	0.015	298.6	0.009	301.0	0.007
725	0.16	207	209.1	0.027	204.0	0.027	203.5	0.027	201.9	0.026	201.2	0.025	207.1	0.028	208.7	0.028
725	0.19	176	195.2	0.011	190.2	0.018	189.8	0.018	188.7	0.019	187.9	0.020	193.3	0.013	194.8	0.012
725	0.23	152	161.0	0.025	156.0	0.031	155.9	0.031	155.1	0.031	154.6	0.032	159.1	0.028	160.0	0.026
725	0.63	371	415.4	0.002	393.1	0.011	394.5	0.010	394.0	0.011	393.5	0.011	407.5	0.004	413.2	0.002
875	0.05	599	590.1	0.015	579.4	0.012	575.5	0.010	566.9	0.007	564.0	0.006	575.8	0.010	582.8	0.013
875	0.07	497	517.7	0.012	506.4	0.016	504.1	0.017	496.5	0.018	494.1	0.018	506.7	0.016	512.2	0.014
875	0.09	407	440.9	0.005	430.2	0.010	428.8	0.011	422.7	0.015	421.2	0.015	433.4	0.009	437.4	0.007
875	0.11	351	357.4	0.020	348.5	0.021	347.5	0.021	343.3	0.019	342.3	0.019	352.7	0.021	355.5	0.021
875	0.14	288	313.2	0.008	305.6	0.014	304.9	0.015	302.0	0.017	301.1	0.018	310.1	0.011	312.3	0.009
875	0.17	291	297.6	0.022	290.3	0.023	289.7	0.023	287.8	0.023	286.7	0.023	295.1	0.023	297.4	0.022
875	0.21	199	215.2	0.015	209.3	0.022	209.0	0.022	207.9	0.023	207.1	0.024	213.2	0.018	214.6	0.016
875	0.26	185	186.8	0.029	180.3	0.028	180.2	0.028	179.5	0.027	178.8	0.026	184.3	0.029	185.3	0.029
875	0.64	482	500.9	0.013	472.6	0.017	474.4	0.017	474.2	0.017	473.8	0.017	491.9	0.016	499.6	0.013
1025	0.05	433	429.0	0.019	421.5	0.016	418.6	0.015	412.4	0.012	410.4	0.010	418.9	0.015	423.9	0.017
1025	0.07	344	374.5	0.006	366.5	0.011	364.8	0.012	359.4	0.015	357.7	0.017	366.8	0.010	370.7	0.008
1025	0.09	314	337.5	0.010	329.5	0.016	328.4	0.016	323.8	0.019	322.7	0.020	332.0	0.014	334.9	0.012
1025	0.11	275	291.0	0.015	283.9	0.021	283.1	0.021	279.7	0.023	278.9	0.023	287.4	0.018	289.6	0.017
1025	0.14	255	260.1	0.024	253.8	0.025	253.2	0.025	250.9	0.024	250.2	0.024	257.7	0.025	259.5	0.024
1025	0.16	184	183.2	0.029	178.8	0.027	178.4	0.027	177.3	0.026	176.6	0.025	181.9	0.029	183.2	0.029
1025	0.20	190	183.0	0.025	178.2	0.020	177.9	0.019	177.0	0.018	176.3	0.017	181.5	0.024	182.8	0.025
1025	0.27	284	279.4	0.023	269.0	0.016	269.0	0.016	267.9	0.015	267.0	0.014	275.7	0.021	277.3	0.022
1025	0.66	281	312.1	0.005	293.4	0.018	294.7	0.017	294.9	0.017	294.8	0.017	307.0	0.008	312.6	0.005
1200	0.06	377	376.9	0.021	370.0	0.019	367.7	0.018	362.4	0.015	360.5	0.014	368.6	0.019	372.7	0.020
1200	0.07	314	328.5	0.016	321.4	0.021	320.0	0.021	315.4	0.022	314.0	0.022	322.3	0.020	325.5	0.018
1200	0.09	285	304.8	0.012	297.6	0.018	296.6	0.019	292.6	0.021	291.7	0.022	300.3	0.016	302.8	0.014

(Table continued)

TABLE IV. *(Continued)*

Q^2		Data	HERAPDF2.0		CT14		MMHT2014		NNPDF3.1		NNPDF2.3		ABMP16		AMB11	
(GeV^2)	x	n	ν	$P(n\|\nu)$	ν	$P(n\|\nu)$	ν	$P(n\|\nu)$	ν	$P(n\|\nu)$	ν	$P(n\|\nu)$	ν	$P(n\|\nu)$	ν	$P(n\|\nu)$
1200	0.12	325	331.6	0.021	323.7	0.022	322.9	0.022	319.3	0.021	318.4	0.021	328.2	0.022	330.5	0.021
1200	0.15	213	226.7	0.018	221.3	0.023	220.8	0.024	219.1	0.025	218.3	0.026	225.0	0.020	226.5	0.018
1200	0.18	210	212.3	0.027	207.1	0.027	206.7	0.027	205.6	0.026	204.7	0.026	210.9	0.028	212.4	0.027
1200	0.22	143	158.8	0.015	154.3	0.022	154.1	0.022	153.4	0.023	152.8	0.024	157.5	0.017	158.4	0.015
1200	0.29	219	236.9	0.013	226.8	0.024	226.9	0.023	226.2	0.024	225.5	0.025	233.4	0.017	235.1	0.015
1200	0.67	275	267.6	0.022	251.3	0.008	252.6	0.009	252.8	0.009	252.9	0.009	263.9	0.019	269.1	0.022
1400	0.06	262	255.2	0.022	250.3	0.019	249.0	0.018	245.4	0.014	244.2	0.013	250.1	0.019	252.7	0.021
1400	0.08	230	227.5	0.026	222.5	0.023	221.7	0.022	218.5	0.020	217.7	0.019	223.8	0.024	225.7	0.025
1400	0.10	206	215.9	0.022	210.8	0.026	210.2	0.027	207.5	0.028	206.9	0.028	213.3	0.025	214.8	0.023
1400	0.12	197	213.5	0.015	208.5	0.021	208.0	0.021	205.9	0.023	205.4	0.024	211.7	0.017	213.0	0.015
1400	0.16	153	154.1	0.032	150.5	0.032	150.1	0.031	149.1	0.031	148.6	0.030	153.2	0.032	154.2	0.032
1400	0.19	148	147.3	0.033	143.6	0.031	143.3	0.030	142.6	0.030	142.0	0.029	146.4	0.033	147.4	0.033
1400	0.23	107	111.2	0.035	107.8	0.038	107.7	0.038	107.2	0.038	106.8	0.038	110.3	0.037	110.8	0.036
1400	0.30	180	174.9	0.028	166.7	0.018	166.9	0.018	166.5	0.018	165.9	0.017	172.2	0.025	173.7	0.027
1400	0.68	146	161.7	0.015	151.7	0.030	152.6	0.029	152.7	0.028	152.9	0.028	159.9	0.018	163.2	0.013
1650	0.05	288	304.8	0.015	300.1	0.018	297.9	0.020	293.7	0.022	292.2	0.023	298.4	0.020	301.6	0.017
1650	0.07	281	256.5	0.008	251.4	0.004	250.2	0.004	246.7	0.002	245.5	0.002	251.8	0.005	254.2	0.006
1650	0.09	244	238.5	0.024	233.2	0.020	232.4	0.019	229.2	0.016	228.5	0.015	235.2	0.022	236.9	0.023
1650	0.11	223	222.2	0.027	217.2	0.025	216.6	0.024	214.0	0.022	213.4	0.022	220.1	0.026	221.5	0.027
1650	0.14	225	208.0	0.013	203.3	0.009	202.8	0.008	201.1	0.007	200.4	0.006	206.7	0.012	207.9	0.013
1650	0.17	202	194.2	0.024	189.6	0.019	189.2	0.018	188.2	0.017	187.4	0.016	193.3	0.023	194.6	0.024
1650	0.21	147	137.4	0.024	133.6	0.017	133.4	0.017	132.8	0.016	132.3	0.015	136.6	0.022	137.4	0.024
1650	0.26	119	123.1	0.034	118.6	0.036	118.6	0.036	118.1	0.036	117.8	0.036	121.9	0.035	122.5	0.035
1650	0.34	167	153.6	0.017	145.2	0.006	145.5	0.007	145.3	0.007	144.8	0.006	150.8	0.013	152.7	0.016
1650	0.70	115	138.1	0.005	129.9	0.015	130.6	0.014	130.8	0.014	131.2	0.013	137.4	0.005	140.4	0.003
1950	0.06	180	184.0	0.029	180.8	0.030	179.8	0.030	177.2	0.029	176.3	0.029	180.6	0.030	182.3	0.029
1950	0.08	161	157.7	0.030	154.4	0.027	153.8	0.027	151.7	0.024	151.1	0.023	155.4	0.028	156.5	0.029
1950	0.10	161	158.9	0.031	155.5	0.029	155.0	0.028	153.0	0.026	152.6	0.025	157.3	0.030	158.3	0.031
1950	0.12	146	163.2	0.013	159.6	0.018	159.2	0.019	157.7	0.021	157.2	0.022	162.2	0.014	163.0	0.013
1950	0.16	117	118.2	0.037	115.6	0.036	115.3	0.036	114.6	0.036	114.1	0.036	117.8	0.037	118.5	0.036
1950	0.19	94	118.6	0.003	115.6	0.005	115.4	0.005	114.9	0.005	114.4	0.006	118.1	0.003	118.8	0.003
1950	0.23	79	100.1	0.004	96.8	0.008	96.8	0.008	96.4	0.008	96.1	0.009	99.4	0.005	99.9	0.004
1950	0.29	65	72.3	0.034	69.1	0.044	69.2	0.043	69.0	0.044	68.8	0.044	71.4	0.037	72.0	0.035
1950	0.37	85	94.1	0.027	88.1	0.041	88.4	0.040	88.5	0.040	88.1	0.041	92.2	0.032	93.8	0.028
1950	0.72	62	71.0	0.028	67.2	0.041	67.5	0.040	67.7	0.040	68.0	0.039	71.3	0.027	72.9	0.021
2250	0.06	135	132.7	0.034	130.8	0.032	129.9	0.031	128.1	0.029	127.4	0.027	130.3	0.032	131.4	0.033
2250	0.07	122	119.5	0.035	117.3	0.033	116.8	0.032	115.2	0.030	114.7	0.029	117.8	0.034	118.6	0.034
2250	0.09	114	110.8	0.036	108.5	0.033	108.1	0.032	106.7	0.029	106.3	0.029	109.6	0.034	110.2	0.035
2250	0.12	134	131.8	0.034	129.1	0.031	128.7	0.031	127.3	0.029	126.9	0.028	131.0	0.033	131.6	0.034
2250	0.15	81	97.5	0.010	95.4	0.014	95.2	0.014	94.5	0.016	94.2	0.017	97.2	0.011	97.7	0.010
2250	0.18	83	94.1	0.022	91.9	0.028	91.7	0.029	91.2	0.030	90.9	0.031	93.8	0.023	94.4	0.021
2250	0.22	51	67.8	0.006	65.8	0.009	65.8	0.009	65.5	0.010	65.2	0.010	67.5	0.006	67.8	0.006
2250	0.27	66	60.6	0.039	58.2	0.030	58.3	0.030	58.1	0.029	57.9	0.028	60.0	0.037	60.4	0.038
2250	0.32	30	44.4	0.005	42.0	0.011	42.1	0.011	42.0	0.011	41.9	0.011	43.7	0.006	44.2	0.005
2250	0.40	53	56.8	0.048	52.8	0.055	53.1	0.055	53.1	0.055	52.9	0.055	55.6	0.051	56.7	0.048
2250	0.73	31	40.0	0.024	38.2	0.035	38.4	0.034	38.5	0.033	38.7	0.031	40.6	0.021	41.5	0.017
2600	0.09	110	110.6	0.038	108.5	0.038	108.1	0.037	106.6	0.036	106.3	0.036	109.4	0.038	110.0	0.038
2600	0.11	111	104.9	0.032	102.8	0.028	102.6	0.027	101.4	0.024	101.1	0.024	104.3	0.031	104.8	0.032
2600	0.14	110	103.8	0.032	101.7	0.027	101.5	0.027	100.6	0.025	100.3	0.024	103.5	0.031	104.0	0.032
2600	0.16	87	81.0	0.034	79.2	0.030	79.1	0.029	78.6	0.028	78.3	0.027	80.9	0.034	81.3	0.035
2600	0.20	65	79.9	0.011	77.9	0.016	77.8	0.016	77.4	0.017	77.1	0.018	79.7	0.011	80.2	0.011
2600	0.24	71	68.6	0.045	66.2	0.040	66.2	0.040	66.0	0.039	65.7	0.038	68.2	0.045	68.5	0.045

(Table continued)

TABLE IV. *(Continued)*

Q^2		Data	HERAPDF2.0		CT14		MMHT2014		NNPDF3.1		NNPDF2.3		ABMP16		AMB11	
(GeV^2)	x	n	ν	$P(n\|\nu)$	ν	$P(n\|\nu)$	ν	$P(n\|\nu)$	ν	$P(n\|\nu)$	ν	$P(n\|\nu)$	ν	$P(n\|\nu)$	ν	$P(n\|\nu)$
2600	0.30	41	48.7	0.033	46.4	0.045	46.5	0.044	46.4	0.045	46.2	0.046	48.1	0.035	48.6	0.033
2600	0.35	36	40.9	0.049	38.4	0.061	38.5	0.061	38.5	0.061	38.4	0.062	40.2	0.053	40.9	0.049
2600	0.44	47	40.3	0.034	37.4	0.018	37.6	0.019	37.6	0.020	37.5	0.019	39.6	0.030	40.5	0.035
2600	0.75	27	28.0	0.075	27.0	0.076	27.1	0.076	27.2	0.076	27.4	0.076	28.8	0.072	29.5	0.069
3000	0.10	75	73.2	0.045	71.9	0.043	71.7	0.043	70.8	0.041	70.6	0.040	72.8	0.044	73.1	0.045
3000	0.12	99	80.2	0.005	78.6	0.004	78.5	0.003	77.7	0.003	77.4	0.003	79.9	0.005	80.2	0.005
3000	0.16	79	62.0	0.005	60.8	0.004	60.7	0.004	60.2	0.003	60.0	0.003	62.0	0.005	62.2	0.006
3000	0.19	61	64.4	0.047	62.9	0.050	62.8	0.050	62.5	0.050	62.2	0.050	64.3	0.047	64.7	0.046
3000	0.23	48	46.3	0.056	44.9	0.052	44.9	0.052	44.7	0.051	44.5	0.050	46.1	0.055	46.4	0.056
3000	0.28	46	42.5	0.051	40.8	0.042	40.8	0.043	40.7	0.042	40.5	0.041	42.2	0.050	42.5	0.051
3000	0.33	30	35.1	0.049	33.1	0.063	33.2	0.062	33.2	0.062	33.0	0.063	34.6	0.053	35.1	0.049
3000	0.39	13	23.2	0.008	21.5	0.015	21.6	0.015	21.7	0.014	21.6	0.015	22.8	0.009	23.2	0.008
3000	0.48	14	21.7	0.022	20.1	0.038	20.2	0.036	20.2	0.036	20.2	0.036	21.4	0.025	21.9	0.020
3000	0.77	13	14.0	0.106	13.8	0.107	13.8	0.107	13.9	0.107	14.1	0.106	14.7	0.099	15.1	0.095
3500	0.12	100	89.9	0.023	88.3	0.019	88.2	0.019	87.2	0.016	86.9	0.015	89.7	0.022	90.0	0.023
3500	0.15	63	72.2	0.027	70.9	0.032	70.8	0.032	70.2	0.034	69.9	0.035	72.2	0.027	72.5	0.026
3500	0.18	78	72.6	0.037	71.0	0.033	71.0	0.032	70.6	0.031	70.3	0.030	72.7	0.037	73.0	0.038
3500	0.22	45	55.3	0.021	53.8	0.028	53.8	0.028	53.5	0.029	53.3	0.030	55.3	0.021	55.5	0.021
3500	0.27	42	48.8	0.038	46.8	0.048	46.9	0.047	46.7	0.048	46.5	0.049	48.5	0.039	48.7	0.038
3500	0.32	29	33.8	0.052	32.0	0.064	32.0	0.064	32.0	0.064	31.9	0.065	33.4	0.055	33.8	0.052
3500	0.37	26	27.8	0.073	26.0	0.078	26.1	0.078	26.1	0.078	26.0	0.078	27.4	0.075	27.9	0.073
3500	0.43	21	18.4	0.072	17.0	0.056	17.1	0.057	17.1	0.057	17.1	0.057	18.1	0.069	18.5	0.073
3500	0.52	24	17.0	0.023	15.9	0.013	16.0	0.014	16.0	0.014	16.1	0.015	17.0	0.023	17.4	0.027
3500	0.79	11	9.9	0.113	10.0	0.114	10.0	0.114	10.1	0.115	10.2	0.116	10.7	0.119	10.9	0.119
4150	0.11	55	56.0	0.053	55.2	0.054	55.1	0.054	54.4	0.053	54.2	0.053	56.0	0.053	56.1	0.053
4150	0.14	54	57.0	0.050	56.1	0.052	56.0	0.052	55.5	0.053	55.3	0.053	57.1	0.050	57.2	0.049
4150	0.17	67	59.5	0.031	58.5	0.027	58.4	0.027	58.0	0.025	57.8	0.024	59.8	0.032	60.0	0.033
4150	0.21	53	46.7	0.036	45.5	0.030	45.5	0.030	45.2	0.029	45.1	0.028	46.7	0.036	46.9	0.037
4150	0.26	34	42.5	0.027	41.0	0.036	41.0	0.036	40.9	0.037	40.7	0.038	42.4	0.028	42.6	0.027
4150	0.31	21	29.9	0.020	28.4	0.030	28.5	0.029	28.4	0.030	28.3	0.031	29.6	0.021	30.0	0.019
4150	0.36	23	23.3	0.083	21.8	0.080	21.9	0.081	21.9	0.081	21.8	0.080	22.9	0.083	23.4	0.083
4150	0.42	16	16.7	0.098	15.5	0.098	15.6	0.099	15.6	0.099	15.6	0.099	16.5	0.099	16.9	0.097
4150	0.48	9	9.5	0.130	8.8	0.131	8.8	0.132	8.8	0.132	8.8	0.132	9.4	0.131	9.6	0.129
4150	0.57	12	8.6	0.062	8.1	0.051	8.2	0.053	8.2	0.052	8.2	0.054	8.8	0.067	9.0	0.072
4150	0.81	6	3.9	0.101	4.2	0.114	4.2	0.113	4.2	0.116	4.3	0.119	4.5	0.127	4.5	0.130
5250	0.11	60	63.9	0.046	63.3	0.047	63.2	0.047	62.3	0.049	62.1	0.050	64.1	0.045	64.1	0.045
5250	0.14	74	67.9	0.036	67.1	0.033	67.1	0.033	66.4	0.030	66.1	0.029	68.3	0.037	68.3	0.037
5250	0.16	60	57.7	0.049	56.8	0.047	56.8	0.047	56.4	0.046	56.1	0.045	58.1	0.050	58.2	0.050
5250	0.20	50	62.0	0.016	60.7	0.021	60.7	0.021	60.3	0.022	60.1	0.023	62.3	0.015	62.4	0.015
5250	0.24	66	57.9	0.028	56.0	0.021	56.0	0.021	55.8	0.020	55.6	0.020	57.9	0.028	58.0	0.029
5250	0.30	36	41.5	0.045	39.5	0.056	39.6	0.056	39.5	0.056	39.4	0.057	41.3	0.047	41.7	0.044
5250	0.35	33	32.4	0.069	30.4	0.062	30.5	0.063	30.5	0.063	30.4	0.062	32.0	0.068	32.6	0.069
5250	0.41	13	21.1	0.018	19.6	0.031	19.7	0.030	19.7	0.030	19.6	0.030	20.9	0.020	21.3	0.017
5250	0.47	13	13.5	0.109	12.5	0.109	12.6	0.109	12.6	0.109	12.6	0.109	13.4	0.109	13.7	0.108
5250	0.53	12	8.3	0.056	7.8	0.044	7.9	0.045	7.9	0.045	7.9	0.046	8.4	0.059	8.7	0.065
5250	0.62	13	7.1	0.016	7.1	0.015	7.1	0.015	7.1	0.015	7.2	0.017	7.6	0.023	7.8	0.026
5250	0.84	3	2.0	0.182	2.3	0.204	2.3	0.203	2.4	0.207	2.4	0.209	2.5	0.212	2.5	0.214
7000	0.12	45	36.5	0.024	36.4	0.023	36.4	0.023	35.9	0.021	35.8	0.020	37.0	0.026	36.8	0.025
7000	0.15	34	36.9	0.061	36.6	0.062	36.6	0.062	36.2	0.064	36.1	0.064	37.3	0.059	37.2	0.059
7000	0.18	40	42.4	0.059	41.8	0.060	41.9	0.060	41.5	0.061	41.4	0.062	42.8	0.057	42.8	0.057
7000	0.22	37	34.5	0.060	33.7	0.056	33.8	0.056	33.6	0.055	33.5	0.055	34.8	0.061	34.8	0.061

(Table continued)

TABLE IV. *(Continued)*

Q^2		Data	HERAPDF2.0		CT14		MMHT2014		NNPDF3.1		NNPDF2.3		ABMP16		AMB11	
(GeV^2)	x	n	ν	$P(n\|\nu)$	ν	$P(n\|\nu)$	ν	$P(n\|\nu)$	ν	$P(n\|\nu)$	ν	$P(n\|\nu)$	ν	$P(n\|\nu)$	ν	$P(n\|\nu)$
7000	0.27	28	33.0	0.050	31.8	0.059	31.9	0.059	31.7	0.060	31.6	0.060	33.0	0.050	33.2	0.049
7000	0.32	27	28.4	0.074	26.9	0.076	26.9	0.076	26.9	0.076	26.8	0.076	28.2	0.074	28.6	0.073
7000	0.38	13	19.6	0.031	18.2	0.048	18.3	0.046	18.4	0.046	18.3	0.047	19.4	0.033	19.8	0.029
7000	0.44	5	11.8	0.015	10.9	0.024	10.9	0.023	11.0	0.023	10.9	0.023	11.7	0.015	11.9	0.013
7000	0.50	10	7.4	0.084	6.9	0.068	7.0	0.070	7.0	0.070	7.0	0.070	7.5	0.085	7.7	0.090
7000	0.56	6	4.4	0.126	4.3	0.117	4.3	0.118	4.3	0.117	4.3	0.120	4.6	0.132	4.7	0.137
7000	0.66	1	3.6	0.101	3.7	0.090	3.7	0.091	3.7	0.091	3.8	0.086	4.0	0.074	4.1	0.069
7000	0.86	0	0.6	0.554	0.8	0.469	0.8	0.474	0.8	0.450	0.8	0.455	0.8	0.450	0.8	0.447
9500	0.17	19	22.5	0.068	22.5	0.069	22.5	0.068	22.3	0.071	22.2	0.071	23.0	0.063	22.9	0.064
9500	0.21	24	23.1	0.080	22.8	0.079	22.8	0.079	22.6	0.078	22.6	0.078	23.4	0.081	23.4	0.081
9500	0.26	23	22.4	0.082	21.8	0.080	21.8	0.080	21.7	0.080	21.6	0.079	22.6	0.083	22.6	0.083
9500	0.31	15	17.1	0.089	16.4	0.097	16.4	0.096	16.4	0.097	16.3	0.097	17.1	0.089	17.3	0.087
9500	0.36	14	15.8	0.096	14.8	0.104	14.9	0.103	14.9	0.103	14.8	0.104	15.7	0.097	16.0	0.093
9500	0.42	9	10.1	0.124	9.4	0.131	9.4	0.130	9.4	0.130	9.4	0.131	10.1	0.124	10.3	0.121
9500	0.48	8	6.4	0.117	6.0	0.103	6.0	0.104	6.0	0.104	6.0	0.104	6.5	0.118	6.7	0.123
9500	0.54	7	3.6	0.044	3.5	0.037	3.5	0.038	3.5	0.037	3.5	0.038	3.8	0.049	3.9	0.053
9500	0.60	2	2.3	0.266	2.3	0.266	2.3	0.266	2.3	0.266	2.3	0.265	2.5	0.259	2.5	0.255
9500	0.71	0	1.4	0.254	1.5	0.214	1.5	0.218	1.5	0.216	1.6	0.207	1.6	0.193	1.7	0.187
9500	0.89	0	0.1	0.865	0.2	0.814	0.2	0.817	0.2	0.797	0.2	0.806	0.2	0.805	0.2	0.805
15500	0.43	41	42.5	0.060	40.7	0.062	40.8	0.062	40.7	0.062	40.5	0.062	43.0	0.059	43.6	0.057
15500	0.80	3	2.5	0.215	2.8	0.222	2.7	0.221	2.8	0.222	2.8	0.222	2.9	0.224	3.0	0.224

APPENDIX B: TABLE OF EFFECT OF LUMINOSITY UNCERTAINTY

TABLE V. The results from comparisons of predictions using different PDF sets increased by 1.8% (top) and decreased by 1.8% (bottom) with respect to the observed numbers of events. The Bayes factor (P1/P2) and $\Delta\chi^2$ (calculated relative to the respective values for the given PDFs as given in Table II) are shown for the two different x ranges defined in the text for the e^-p and e^+p data sets.

	e^-p				e^+p			
	Lower x		Higher x		Lower x		Higher x	
PDF	P1/P2	$\Delta\chi^2$	P1/P2	$\Delta\chi^2$	P1/P2	$\Delta\chi^2$	P1/P2	$\Delta\chi^2$
				+1.8%				
HERAPDF2.0	1.7×10^{-3}	13	0.08	5.0	8.6×10^{-5}	19	0.01	9.8
CT14	28	−6.7	16	−5.5	5.0×10^{-2}	6.0	0.37	2.0
MMHT2014	$1.1 \times 10^{+2}$	−9.5	13	−5.1	0.11	4.4	0.31	2.3
NNPDF3.1	$4.9 \times 10^{+3}$	−17	15	−5.4	2.2	−1.5	0.36	2.0
NNPDF2.3	$1.8 \times 10^{+4}$	−20	18	−5.8	5.9	−3.6	0.41	1.8
ABMP16	0.37	2.0	0.30	2.4	2.6×10^{-3}	12	0.02	7.8
ABM11	9.6×10^{-3}	9.3	0.07	5.3	2.9×10^{-4}	16	0.01	10
				−1.8%				
HERAPDF2.0	0.69	0.74	1.7	−1.1	93	−9.1	30	−6.8
CT14	4.9×10^{-5}	20	9.3×10^{-3}	9.3	0.18	3.4	0.66	0.83
MMHT2014	1.2×10^{-5}	23	1.1×10^{-2}	8.9	8.0×10^{-2}	5.0	0.77	0.51
NNPDF3.1	3.1×10^{-7}	30	9.8×10^{-3}	9.3	4.4×10^{-3}	11	0.67	0.79
NNPDF2.3	8.5×10^{-8}	33	8.2×10^{-3}	9.6	1.6×10^{-3}	13	0.59	1.1
ABMP16	3.5×10^{-3}	11	0.46	1.5	3.3	−2.4	12	−4.9
ABM11	0.12	4.2	1.9	−1.3	28	−6.6	33	−7.0

APPENDIX C: TABLES OF SELECTION FOR INCLUSION OF HIGH-x DATA IN PDF EXTRACTIONS

TABLE VI. List of $e^{\pm}p$ combined data points [9] to be removed and the ZEUS high-x data points [8] to be added. See Sec. VI for details.

HERA combined points to be removed	
x	Q^2 (GeV^2)
0.4	1200 1500 2000 3000 20000
0.6	3000 8000

ZEUS high-x data to be added	
x	Q^2 (GeV^2)
Integrated	725 875 1025 1200 1400 1650 1950 2250 2600 3000 3500 4150 5250 7000 9500
0.37	1950
0.4	2250
0.35, 0.44	2600
0.39, 0.48	3000
0.57	4150
0.53, 0.62	5250
0.56, 0.66	7000
0.54, 0.61, 0.71	9500
0.8	15500

TABLE VII. Luminosity reduction factors for ZEUS high-x data and cross section enhancement factors for H1 data to adjust to normalization shifts applied during data combination.

	e^-p	e^+p
ZEUS luminosity reduction factor	0.987	0.975
H1 cross section enhancement factor	1.024	1.013

[1] J. Butterworth *et al.*, J. Phys. G **43**, 023001 (2016).
[2] J. Rojo *et al.*, J. Phys. G **42**, 103103 (2015).
[3] V. N. Gribov and L. N. Lipatov, Sov. J. Nucl. Phys. **15**, 438 (1972).
[4] V. N. Gribov and L. N. Lipatov, Sov. J. Nucl. Phys. **15**, 675 (1972).
[5] L. N. Lipatov, Sov. J. Nucl. Phys. **20**, 94 (1975).
[6] Yu. L. Dokshitzer, Sov. Phys. JETP **46**, 641 (1977), http://www.jetp.ac.ru/cgi-bin/e/index/e/46/4/p641?a=list.
[7] G. Altarelli and G. Parisi, Nucl. Phys. **B126**, 298 (1977).
[8] H. Abramowicz *et al.* (ZEUS Collaboration), Phys. Rev. D **89**, 072007 (2014).
[9] H. Abramowicz *et al.* (H1 and ZEUS Collaborations), Eur. Phys. J. C **75**, 580 (2015).
[10] F. Beaujean, A. Caldwell, D. Kollár, and K. Kröninger, Phys. Rev. D **83**, 012004 (2011).
[11] A. Kwiatkowski, H. Spiesberger, and H.-J. Möhring, Comput. Phys. Commut. **69**, 155 (1992); Also in *Proc. Workshop Physics at HERA*, edited by W. Buchmüller and G. Ingelman (DESY, Hamburg, 1991).
[12] H. L. Lai, J. Huston, S. Kuhlmann, J. Morfin, F. Olness, J. F. Owens, J. Pumplin, and W. K. Tung (CTEQ Collaboration), Eur. Phys. J. C **12**, 375 (2000).
[13] L. Lönnblad, Comput. Phys. Commun. **71**, 15 (1992).
[14] G. Ingelman, A. Edin, and J. Rathsman, Comput. Phys. Commun. **101**, 108 (1997).
[15] R. Brun *et al.*, GEANT3, CERN Technical Report No. CERN-DD/EE/84-1, 1987.
[16] S. Dulat, T.-J. Hou, J. Gao, M. Guzzi, J. Huston, P. Nadolsky, J. Pumplin, C. Schmidt, D. Stump, and C.-P. Yuan, Phys. Rev. D **93**, 033006 (2016).
[17] L. Harland-Lang, A. D. Martin, P. Motylinski, and R. Thorne, Eur. Phys. J. C **75**, 204 (2015).
[18] R. D. Ball *et al.*, Eur. Phys. J. C **77**, 663 (2017).
[19] R. D. Ball *et al.*, Nucl. Phys. **B867**, 244 (2013).
[20] S. Alekhin, J. Blümlein, S. Moch, and R. Plačakytė, Phys. Rev. D **96**, 014011 (2017).
[21] S. Alekhin, J. Blümlein, and S. Moch, Phys. Rev. D **86**, 054009 (2012).
[22] R. Aggarwal and A. Caldwell, Eur. Phys. J. Plus **127**, 24 (2012).

[23] H. Abramowicz *et al.* (ZEUS Collaboration), Phys. Rev. D **87**, 052014 (2013).
[24] S. Chekanov *et al.* (ZEUS Collaboration), Eur. Phys. J. C **62**, 625 (2009).
[25] F. D. Aaron *et al.* (H1 Collaboration), J. High Energy Phys. 09 (2012) 061.
[26] F. D. Aaron *et al.* (H1 and ZEUS Collaborations), J. High Energy Phys. 01 (2010) 109.
[27] See Supplemental Material at http://link.aps.org/supplemental/10.1103/PhysRevD.101.112009 for the PDF sets ABMP16, AMB11, NNPDF3.1, NNPDF2.3, CT14, and MMHT2014.